Vaccination with mycobacterial lipid loaded nanoparticle leads to lipid antigen persistence and memory differentiation of antigen-specific T cells

Eva Morgun,[1] Jennifer Zhu,[2] Sultan Almunif,[2] Sharan Bobbala,[2, †], Melissa S. Aguilar,[3] Junzhong Wang, [1, ‡] Kathleen Conner, [1] Yongyong Cui, [1] Liang Cao,[1] Chetan Seshadri,[3] Evan A. Scott,[1,2]* Chyung-Ru Wang[1]*

[1]Department of Microbiology and Immunology, Feinberg School of Medicine, Northwestern University, Chicago, IL, USA

[2]Department of Biomedical Engineering, Northwestern University, Evanston, IL, USA

[3]Department of Medicine, University of Washington School of Medicine, Seattle, WA, USA

Present addresses

[†] Department of Pharmaceutical Sciences, School of Pharmacy, West Virginia University, Morgantown, WV, USA

[‡]Department of Infectious Disease, Union Hospital of Tongji Medical College, Huazhong University of Science and Technology, Wuhan, China

***Corresponding authors:** Dr. Chyung-Ru Wang (chyung-ru-wang@northwestern.edu)
Dr. Evan A Scott (evan.scott@northwestern.edu)

Running title: Nanoparticle encapsulated lipid elicits antigen persistence

Keywords: nanoparticle, antigen persistence, CD1, mycolic acid, T cell, vaccination, *Mycobacterium tuberculosis*

Abstract

Mycobacterium tuberculosis (Mtb) infection elicits both protein and lipid antigen-specific T cell responses. However, the incorporation of lipid antigens into subunit vaccine strategies and formulations has been underexplored, and the characteristics of vaccine-induced Mtb lipid-specific memory T cells have remained elusive. Mycolic acid (MA), a major lipid component of the Mtb cell wall, is presented by human CD1b molecules to unconventional T cell subsets. These MA-specific CD1b-restricted T cells have been detected in the blood and disease sites of Mtb-infected individuals, suggesting that MA is a promising lipid antigen for incorporation into multicomponent subunit vaccines. In this study, we utilized the enhanced stability of bicontinuous nanospheres (BCN) to efficiently encapsulate MA for *in vivo* delivery to MA-specific T cells, both alone and in combination with an immunodominant Mtb protein antigen (Ag85B). Pulmonary administration of MA-loaded BCN (MA-BCN) elicited MA-specific T cell responses in humanized CD1 transgenic mice. Simultaneous delivery of MA and Ag85B within BCN activated both MA- and Ag85B-specific T cells. Notably, pulmonary vaccination with MA-Ag85B-BCN resulted in the persistence of MA, but not Ag85B, within alveolar macrophages in the lung. Vaccination of MA-BCN through intravenous or subcutaneous route, or with attenuated Mtb likewise reproduced MA persistence. Moreover, MA-specific T cells in MA-BCN-vaccinated mice differentiated into a T follicular helper-like phenotype. Overall, the BCN platform allows for the dual encapsulation and *in vivo* activation of lipid and protein antigen-specific T cells and leads to persistent lipid depots that could offer long-lasting immune responses.

48 **Introduction**

49

50 Vaccination is currently the most effective method for the prevention and eradication of
51 infectious diseases. These efforts have been enhanced by the development of subunit vaccine
52 formulations that include only immunodominant antigens from pathogens paired with select adjuvants.
53 In contrast to attenuated and inactivated vaccines that contain diverse molecular components of
54 pathogens, subunit vaccines are often preferred due to their simplicity, safety, stability, and scalability
55 of production [1]. Yet the development of effective vaccines for several key endemic parasitic and
56 bacterial pathogens has remained elusive. Antigen selection for subunit vaccines has thus far focused
57 on protein molecules, overlooking a vast family of non-protein antigens such as lipids/glycolipids,
58 metabolites, and phosphoantigens, which can be found on and within pathogens and can be recognized
59 by various subsets of unconventional T cells [2].

60 Persistent antigen exposure is known to occur naturally after infection through antigen
61 archiving by follicular dendritic cells (FDCs), which periodically present antigen to cognate B cells
62 and aid in affinity maturation and somatic hypermutation [3, 4]. Antigen persistence can also support
63 the maintenance of T cell response through the periodic priming of circulating T cells [5-10].
64 Subcutaneous vaccination has also been shown to lead to archiving of protein antigens within
65 lymphatic endothelial cells (LECs), which induce the development of protective T cell immunity [11,
66 12]. However, little is known about how other vaccination routes and vaccine formulations may affect
67 antigen archiving and persistence.

68 Lipid and glycolipid antigens can be presented by group 1 (CD1a, b, and c) and group 2
69 (CD1d) CD1 molecules to CD1-restricted T cells. Unlike MHC molecules, CD1 molecules exhibit
70 limited polymorphism [13]. Therefore, CD1-restricted microbial lipid antigens are likely to be
71 recognized by most individuals, making them attractive targets for vaccine development [14]. Group 1
72 CD1-restricted T cells have diverse T cell receptors and can recognize a variety of lipid and glycolipid
73 antigens [15]. Microbial lipid-specific group 1 CD1-restricted T cells have been identified from several
74 pathogens, including Mtb and other mycobacterial species: *Staphylococcus aureus* (SA), *Borrelia*

75 *burgdorferi*, *Salmonella typhimurium*, and *Brucella melitensis* [15]. CD1b-restricted T cells specific to
76 Mtb lipids including mycolic acid (MA), an immunodominant lipid antigen[16] and component of the
77 mycobacterial cell wall, have been identified in patients with tuberculosis (TB) [17, 18]. As group 1
78 CD1 molecules are not expressed in mice, we have previously developed a human CD1 transgenic
79 mouse model (hCD1Tg). [19] Using hCD1Tg mice, we have shown that transgenic CD1b-restricted
80 DN1 T cells specific for MA could protect against Mtb infection [20], making these potential antigens
81 of interest in a subunit vaccine against TB.

82 The primary goal of a vaccine is to induce the differentiation of the adaptive immune system
83 such that upon re-exposure to the antigen, a faster and larger response occurs, halting pathogen spread.
84 While conventional T cells and B cells are known to undergo this differentiation, unconventional T
85 cells such as NKT cells do not possess a comparable memory phenotype. The presence of Mtb lipid-
86 specific group 1 CD1-restricted memory T cells has been described in both human and mice [17-19].
87 However, the properties of memory group 1 CD1-restricted T cells, which share similar developmental
88 pathway as NKT cells, are not known.

89 Lipid antigens are difficult to formulate and administer due to their hydrophobic nature. To
90 assess the utility of MA as a component of a subunit vaccine, we previously encapsulated MA in
91 poly(ethylene glycol)-block-poly(propylene sulfide) (PEG-*b*-PPS) micellar nanocarriers (MA-MC)
92 [21]. Nanocarriers composed of PEG-*b*-PPS possess several unique benefits compared to other
93 delivery platforms, including high stability in aqueous solution [22], minimal background
94 immunostimulation [23], and triggered release of cargo when exposed to physiological levels of
95 reactive oxygen species [24-26]. We showed MA-MC could effectively activate adoptively transferred
96 DN1 T cells and elicit polyclonal group 1 CD1-restricted T cell response in hCD1Tg mice after
97 intranasal delivery [21]. While effective for stable loading of lipophilic and amphiphilic payloads,
98 micellar nanocarriers, do not allow for facile encapsulation of hydrophilic payloads like protein
99 antigens.

100 Here, we build upon our prior lipid antigen vaccine formulation by employing a nanocarrier
101 platform engineered for the dual loading of both lipid and protein antigens. Bicontinuous nanospheres

102 (BCN) are polymeric analogs to lipid cubosomes and thus possess a highly organized internal cubic
103 organization containing both intertwined hydrophobic bilayers for lipid loading as well as hydrophilic
104 aqueous channels for protein loading [27]. Using the flash nanoprecipitation (FNP) technique [28, 29],
105 we fabricated MA-loaded BCN (MA-BCN) and found them to have superior stimulatory capacity *in*
106 *vivo* compared to MA loaded poly(D,L-lactide-co-glycolide) (PLGA) nanocarriers (MA-PLGA),
107 which is a widely used nanocarrier platform for Mtb vaccine development [30, 31]. Furthermore, we
108 found that after MA-BCN vaccination, MA could persist for 6 weeks post-vaccination within alveolar
109 macrophages, a phenomenon which was dependent on the presence of an encapsulating vector,
110 nanocarrier or bacterial, but not the route of vaccination. Due to the enhanced stability of the BCN
111 architecture that can support the loading of diverse and multiple payloads [22, 32], we were able to
112 efficiently co-encapsulate within BCN both MA and Ag85B, an immunodominant protein antigen of
113 Mtb [33]. Interestingly, while both antigens activated their corresponding antigen-specific T cells,
114 only MA resulted in antigen persistence, suggesting a potentially unique characteristic of subunit
115 vaccines containing lipid antigens.

116 **Results**

117

118 **BCN morphology preserved after MA loading**

119 We scalably assembled spherical BCN with and without loaded MA using flash
120 nanoprecipitation (FNP) as previously described [29]. Dynamic light scattering (DLS) showed that
121 both MA-BCN and BCN were consistent in size (364 ±19 nm and 354 ± 14 nm, respectively), and
122 were monodisperse based on their polydispersity indices (PDIs) of 0.24 ± 0.04 and 0.21 ±0.05,
123 respectively (**Fig 1A**). We next verified that the BCN formulation maintained its characteristic
124 interconnected aqueous channels using cryogenic transmission electronic microscopy (cryo-TEM) (**Fig**
125 **1B**) and negative staining transmission electron microscopy (TEM) (**Fig 1C**). Using small angle X-ray
126 scattering (SAXS) studies, we confirmed the internal cubic organization of BCN. Bragg peaks at the
127 √2, √4, and √6 ratios show that the primitive type of cubic internal organization was preserved between
128 MA-BCNs and BCNs (**Fig 1D**). Thus, MA encapsulation did not disturb the BCN architecture. We
129 also manufactured a PLGA nanocarrier formulation (PLGA-NP) with and without MA encapsulation.
130 PLGA-NP morphology were confirmed using cryoTEM (**Suppl Fig 1A**) and SAXS (**Suppl Fig 1B**)
131 and the size of blank PLGA-NP and MA-loaded PLGA-NP (MA-PLGA) were found to be 169 ± 4 and
132 163 ± 5 nm, respectively, with PDIs of 0.18 ± 0.04 and 0.19 ± 0.12, respectively (**Fig 1E**). Using the
133 coumarin derivatization method [21], we found that BCNs could more efficiently encapsulate MA than
134 PLGA-NPs (**Fig 1F**). We previously noted that the highly stable cubic architecture of BCN can lead to
135 the retention of cargo within the endolysosomal compartment [22]. Indeed, Texas Red-Dextran loaded
136 BCN were mostly found in lysosomes while Texas Red-Dextran loaded PLGA-NP could be found
137 both within the lysosome and cytosol of cells (**Supp Fig 2A, B**).

138

139 **MA-BCN activate MA-specific T cells *in vitro* and *in vivo***

140 As PLGA has served as a component of a wide range of vaccine formulations, including Mtb
141 vaccines [30, 31], we benchmarked PEG-*b*-PPS BCN against PLGA-NP as a nanocarrier platform for
142 lipid antigens. Both MA-BCN and MA-PLGA were highly effective in activating both mouse (DN1)

143 and human (M11) MA-specific T cells *in vitro* and inducing IFN-γ production (**Fig 2A-D**). In
144 particular, MA-BCN were significantly better at activating MA-specific T cells compared to free MA
145 at equivalent concentrations (**Fig 2A, B and D**). In comparison to MA-BCN, MA-PLGA was
146 significantly more effective at stimulating mouse MA-specific T cells *in vitro* at lower concentrations.
147 Interestingly, even in the absence of MA, PLGA-NP showed strong stimulation particularly for M11 T
148 cells. These results demonstrate that MA encapsulation within BCN enhances its ability to stimulate
149 antigen-specific T cells and reveal a considerable background, and thus difficult to control, stimulatory
150 effect of blank PLGA-NP. In contrast, blank BCN showed little background immunostimulation [23],
151 allowing a more controlled dose-dependent increase in T cell responses as the loaded MA
152 concentration increased.

153 We next tested the ability of MA-loaded and unloaded BCN and PLGA to stimulate DN1 T
154 cells *in vivo*. Intranasal (IN) vaccination of hCD1Tg mice was followed by the adoptive transfer of
155 DN1 T cells. Surprisingly, we found that vaccination with MA-BCN induced a significantly higher
156 percent of proliferation and activation in DN1 T cells than MA-PLGA in the draining lymph nodes
157 (LN) and lungs at 1 week post-vaccination (**Fig 2E-G**). The extent of cell proliferation induced by
158 MA-PLGA was not significantly different from that of blank PLGA (**Fig 2F**). Since MA-BCN
159 effectively stimulated MA-specific T cells *in vivo* while MA-PLGA did not, we focused on further
160 characterizing and assessing vaccination via solely MA-BCN formulations.

161

162 **MA persists while Ag85B does not after vaccination with Ag85B-MA-BCN**

163 Given the lack of knowledge regarding BCN and lipid antigen kinetics, it would be of interest
164 to test whether delivered antigen could persist in the mouse weeks post-vaccination (**Fig 3A**). We
165 switched from intranasal vaccination to intratracheal (IT) vaccination, as it allowed for the reliable
166 delivery of a larger volume of the vaccine. We found that a significant proportion of the adoptively
167 transferred DN1 T cells could proliferate and become activated in the LNs, lung, and spleen of MA-
168 BCN-vaccinated mice 6 weeks post vaccination (**Fig 3B-D**). This activation and proliferation were

169 MA-specific, as no activation and proliferation of Ag85B-specific p25 Tg (p25) T cells were
170 observed[34].

171 Since BCN allow for the co-loading of lipid and protein antigens, we assessed the ability of
172 dual loaded Ag85B-MA-BCN to activate antigen-specific T cells as well as lead to antigen persistence.
173 We co-loaded Ag85B and MA in BCN and found Ag85B-MA-BCN to have a diameter of 380 nm and
174 PDI of 0.223, comparable to MA-BCN (**Fig 4A**). Encapsulation efficiency was also relatively high at
175 70%.Vaccination of hCD1Tg mice with Ag85B-MA-BCN activated and induced proliferation of both
176 p25 and DN1 T cells in the LN, lung, and spleen (**Fig 4B-D**) at one-week post-vaccination. In addition,
177 DN1 T cells were still able to be activated 6 weeks post-vaccination in the context of an Ag85B-MA-
178 BCN vaccination, while p25 T cells did not show increased activation or proliferation compared to
179 blank BCN control at this time point (**Fig 4E-H**). Therefore, MA, but not Ag85B, appears to persist in
180 the context of an Ag85B-MA-BCN vaccination.

181

182 **MA persistence was dependent on encapsulation but not route of delivery or delivery vector**

183 To determine whether BCN encapsulation contributed to MA persistence, we designed an
184 experiment that would allow direct comparison between MA-BCN and free MA. To account for their
185 differential efficiency in stimulating DN1 T cells, we pulsed bone marrow-derived dendritic cells
186 (BMDCs) from hCD1Tg mice with MA or MA-BCN at 10 μg/mL and 5 μg/mL MA concentration,
187 respectively (**Fig 5A**). hCD1Tg mice were immunized with MA or MA-BCN-pulsed BMDCs at either
188 1 week or 6 weeks before the adoptive transfer of DN1 T cells, allowing comparison of short-term *vs.*
189 long-term vaccination conditions. We found that while there were no significant differences in DN1 T
190 cell activation and proliferation between mice vaccinated with free MA and MA-BCN pulsed BMDCs
191 at 1-week post-vaccination, after 6 weeks, DN1 T cell response could only be detected in the MA-BCN
192 vaccination condition (**Fig 5B, C**). Thus, BCN encapsulation contributed to the persistence of MA. We
193 then tested whether the BCN structure could contribute to antigen persistence by comparing PEG-*b*-
194 PPS BCNs to PEG-*b*-PPS MCs using a similar experimental set up (**Suppl Fig 3**). We found that MA-
195 BCN and MA-MC overall had similar ability to activate DN1 T cells in both short-term and long-term

196 vaccination time points (**Suppl Fig 3B, C**). Thus, the structure of the encapsulating NP did not play a
197 significant role in antigen persistence of MA.

198 To investigate if the IT route of vaccination played a role in the development of antigen
199 persistence, we tested intravenous (IV) and subcutaneous (SC) vaccination routes with MA-BCN. DN1
200 T cell activation and proliferation were detected at 6-weeks post-vaccination through both routes of
201 vaccination (**Fig 5D-F**), suggesting that the antigen persistence is not unique to IT vaccination. To
202 assess whether Mtb lipid antigen persistence could also be observed in mice vaccinated with an
203 attenuated strain of Mtb, we vaccinated hCD1Tg mice SC with Mtb $mc^2$6206 strain and tested for the
204 persistence of both Ag85B and MA after 6 weeks. The Mtb $mc^2$6206 strain displays less virulence in
205 mouse studies than BCG but still confers long-term protection against virulent Mtb challenge
206 equivalent to BCG[35]. We confirmed that no bacterial burden remained at the 6 weeks time point
207 (**Suppl Fig 4A**). Similar to MA-BCN-vaccinated mice, DN1 T cells were activated and proliferated in
208 the draining lymph nodes and spleen of mice vaccinated with the attenuated Mtb strain (**Fig 5D-F**). In
209 line with our findings with BCN, no proliferation was seen in p25 T cells (**Suppl Fig 4B-D**). These
210 results suggest that incorporation of MA in a nanocarrier vaccine allows for the mimicry of the lipid
211 antigen persistence induced by vaccination with an attenuated Mtb vaccine.

212

213 **MA persists within alveolar macrophages in the lung**

214 To identify the location of antigen persistence, we determined the biodistribution of BCN after
215 IT vaccination using BCN loaded with the hydrophobic dye DiD (DiD-BCN). Since DiD is a lipophilic
216 dye which, like MA, stably loads into the BCN bilayers, we could track the localization of BCN
217 without having to perform additional chemical modifications. We found that IT-administered DiD-
218 BCN were located almost exclusively within the lung at all time points tested (4 h, 24 h, 48 h, 6 days,
219 and 6 weeks) (**Fig 6A**). We were able to detect fluorescence through both *in vivo* imaging system
220 (IVIS) and flow cytometry at 6-weeks post-vaccination that was significantly above unvaccinated
221 control (**Fig 6A, B**), despite DiD quickly losing fluorescence upon mixture into aqueous environments
222 [36], suggesting that some DiD-BCN structure remained intact at this time point. Flow cytometric

223 analysis (**Suppl Fig 5**) revealed that DiD BCN was primarily found within alveolar macrophages
224 (AMs) at both early and late time points with neutrophils and DCs showing some fluorescence at early
225 time points (4 and 24 h) (**Fig 6C**).

226 We next tested whether MA likewise persisted primarily within AMs. 6-weeks after
227 vaccination, we enriched for AMs using a column-based magnetic cell isolation system containing
228 SiglecF antibody, which is highly expressed on AMs and a small population of eosinophils in the lung
229 (**Fig 6D**). We co-cultured enriched AMs or the flow through with or without hCD1Tg-expressing
230 BMDCs and DN1 T cells (**Suppl Fig 6**). While both enriched AM and flow through fractions from
231 MA-BCN vaccinated mice co-culture with BMDCs could activate DN1 T cells (**Fig 6E**), co-culture
232 with enriched AMs led to significantly higher DN1 T cell activation, suggesting AMs are the primary
233 location of MA persistence. The ability of flow through to likewise lead to DN1 T cell activation
234 suggests MA may also persist in other cell types or could be attributed to residual AMs in flow
235 through. Furthermore, AMs could not themselves present the MA to DN1 T cells, noted by the lack of
236 T cell activation in the absence of BMDCs, suggesting that MA may be transferred from AMs to DCs
237 for presentation. In fact, CD1b is not expressed on AMs [19, 37] and therefore the presence of CD1b-
238 expressing DCs may be necessary both *in vitro* and *in vivo* for T cell activation to occur. These data
239 indicate that MA-BCN mainly persists within AMs in the lung after IT vaccination and CD1b-
240 expressing DCs is required for antigen presentation and activation of MA-specific T cells.

241

242 **Vaccination leads to DN1 T cell differentiating into T follicular helper-like T cells**

243 To study the memory phenotype of DN1 T cells after MA-BCN vaccination, we constructed a
244 mixed DN1 bone marrow (BM) chimera mouse model (DN1-hCD1Tg), since adoptively transferred
245 DN1 T cells in unvaccinated mice cannot survive long term (**Fig 7A**). After vaccination, the percent of
246 $CD44^+$ DN1 T cells in the blood increased quickly and remained high until the last time point of 40
247 days (**Fig 7B**). Various classical memory T cell subsets have been characterized 1 month after initial
248 antigen-encounter, we therefore determined the DN1 T cell phenotype 6-weeks post vaccination. We
249 found that the most prevalent memory population within DN1 T cells were $CD44^+CD62L^+$, markers

250 used to define central memory T cells, particularly in the LN (**Fig 7C** and **Supp Fig 7A**). To
251 characterize the memory DN1 T cells, we performed RNA-seq analysis on sorted $CD44^{+}CD62L^{+}$
252 (memory) and $CD44^{-}CD62L^{+}$ (naïve) DN1 T cells from LNs of MA-BCN vaccinated DN1-hCD1Tg
253 BM chimeric mice. We found that memory and naïve DN1 T cells clustered separately after principal
254 component analysis (PCA), despite these samples coming from the same animals (**Suppl Fig 7B**). A
255 total of 995 differentially expressed genes (DEGs) were identified of which 542 upregulated and 453
256 downregulated in the memory subset (**Suppl Fig 7C**). Next, we determined which T cell population
257 memory DN1 T cells most resembled. Toward this end, we obtained data from ImmGen database
258 (including terminally differentiated effector (Te), memory precursor (Tmp), central memory (Tcm),
259 effector memory (Tem), regulatory (Treg))[42], and two additional publications (follicular helper (Tfh)[43],
260 exhausted (Texh)[44]) and compared the respective DEG lists. Using PCA, we found that memory DN1
261 T cells clustered most closely to Tfh, Treg, and Texh (**Fig 7D**) and when this subset is isolated, most
262 closely to Tfh cells (**Fig 7E**).

263 Within the DEGs, we noted upregulation of key Tfh cell transcription factors BCL6 and TCF1
264 (*TCF7*), chemokines CXCR5 and CXCR4 and surface receptor ICOS, important for Tfh cell migration
265 into the germinal center, and adaptor protein SAP (*SH2D1A*), important for T cell-dependent B cell
266 immunity (**Fig 7F**)[45]. Inhibitory receptors PD-1 (*PDCD1*), TIGIT, CTLA4, and transcription factor
267 EOMES, which are known to be expressed on Tfh cells were also upregulated. In addition, we
268 observed downregulation of transcription factor KLF2, which can inhibit Tfh cell differentiation, and
269 CCR7 and IL-7R, receptors known to have decreased expression in T_{FH} cells. Consistent with our
270 transcriptome analysis, we found increased percentage of $CXCR5^{+}PD\text{-}1^{+}$ DN1 T cells in MA-BCN
271 vaccinated mice 6 weeks post-immunization (**Fig 7G, H**). Both our transcriptomic and experimental
272 data highlighted that memory, but not naïve DN1 T cells, were proliferating, given the enrichment for
273 the mitotic cell cycle process (**Fig 7I**) and increased $KI67^{+}$ percentage within this population (**Fig 7J**).
274 MA-BCN vaccination thus led to the differentiation of DN1 T cells into a proliferating Tfh-like T cell
275 population.
276

277 **Discussion**

278

279 Research on the development of subunit vaccines containing lipid antigens is limited. This is in
280 part due to a lack of research into appropriate lipid vaccine formulations and their associated
281 properties. Some early evidence suggests that lipid vaccines could contribute to protection in Mtb
282 challenge in guinea pig model [38, 39], which naturally express group 1 CD1 molecules [40].
283 Vaccination with a formulation composed of total Mtb lipid encapsulated within liposomes with either
284 dimethyl-dioctadecyl-ammonium (DDA) and/or QS-21 adjuvants showed lower bacterial burden and
285 pathology in lung and spleen compared to unvaccinated controls [38]. In another study, two Mtb lipids
286 (diacylated sulfoglycolipids and the phosphatidylinositol dimannosides) encapsulated into liposomes
287 formulated with DDA and trehalose 6,6'-dibehenateled (TDM) to a decreased bacterial burden in the
288 spleen and overall improved pathology in lung and spleen [39]. This work motivated our current study,
289 where we used hCD1Tg mice that express human group 1 CD1 molecules, including CD1b and MA-
290 specific (DN1), as well as p25-specific T cells to investigate the use of nanocarriers coloaded with both
291 Mtb lipid and protein antigens during vaccination (**Fig 8**).

292 We found that PEG-*b*-PPS BCN could effectively encapsulate MA as well as the protein
293 antigen Ag85B to elicit activation of antigen-specific T cells in vaccinated mice (**Fig 4**). To our
294 knowledge, this is the first time a dual protein and lipid loaded nanocarrier has been shown to
295 effectively stimulate both lipid and peptide antigen-specific T cells simultaneously *in vivo*. PEG-*b*-PPS
296 BCN can encapsulate both hydrophobic and hydrophilic molecules, making it an excellent platform for
297 subunit vaccine delivery as both antigens and adjuvants can be co-loaded and delivered to the same
298 cellular targets. Prior work on TB vaccines has shown that the inclusion of several protein antigens
299 spanning the Mtb life cycle along with adjuvants with multiple boosts is paramount in the development
300 of a vaccine that can provide effective protection against Mtb [30, 41]. As we have established that
301 PEG-*b*-PPS BCN can easily incorporate a variety of payloads, future work will involve determining
302 the optimal antigen and adjuvant combination for providing protection in a Mtb challenge experiment.

303 As several formulations of PLGA-NP have been approved for clinical uses [42], we compared
304 MA encapsulated by either BCN or PLGA-NP and found that while PLGA appeared to offer greater,
305 yet less controllable stimulation *in vitro* (**Fig 2**), BCN exhibited significantly greater efficacy *in vivo*
306 (**Fig 2**). The result is not completely unexpected as a more fragile PLGA-NP could allow for fast
307 intracellular release and antigen presentation *in vitro* while also leading to significant antigen loss prior
308 to APC interaction *in vivo* (**Fig 3**) [43]. Previous studies have documented PLGA's innate pro-
309 inflammatory effects, while other studies have highlighted the absence and suppression of
310 inflammatory response [44-46]. As PLGA has not been previously used for lipid antigen delivery via
311 IT vaccination, our findings suggest that PLGA may have limited effectiveness in such a vaccine
312 system, although alternative formulations or polymer compositions could potentially yield improved
313 results. In contrast and as previously observed for PEG-*b*-PPS nanocarriers [23], we showed that
314 unloaded BCN have little inflammatory effect (**Fig 2**), allowing their immunomodulation to be dictated
315 by the properties of the loaded antigen and adjuvant. Thus, PEG-*b*-PPS is a promising polymer for the
316 formulation of subunit vaccines.

317 We proceeded with a pulmonary (IN or IT) vaccination approach in this study based on
318 emerging evidence that mucosal vaccination can induce a stronger immune response in the lung
319 against Mtb in humans [47] and improve protection following vaccination with nanocarriers in mice
320 [48]. We found that in the pulmonary route of vaccination, BCN primarily were taken up and remained
321 within alveolar macrophages in the lung (**Fig 6**). In fact, the ability of nanocarriers to target alveolar
322 macrophages or other APCs may contribute to their distinct capacity for inducing antigen persistence,
323 which was not seen with cellular carriers such as MA-pulsed BMDCs (**Fig 5**). Alveolar macrophages
324 are the first line of defense of the lungs, responsible for keeping alveoli sterile by taking up inhaled
325 particles and pathogens through phagocytosis [49-51]. Targeting these cells may be particularly
326 beneficial in a TB vaccine design since they may also be the main site of Mtb latency [52]. While MA
327 remained within alveolar macrophages in the lung, T cell activation appeared to occur prominently
328 within the draining lymph nodes (**Fig 2**), suggesting that either MA was transported from the lungs to
329 lymph nodes where the presentation took place or T cells activated in the lung migrated to the lymph

330 nodes. The first option seems most likely, as CD1b-expressing DCs are more prevalent in the lymph
331 nodes [53]. Furthermore, in Mtb infection models, it has been previously shown that apoptotic
332 macrophage and vesicles could deliver mycobacterial antigens to DCs that then activate cognate T
333 cells [54, 55]. Similarly, we showed that alveolar macrophages from MA-BCN vaccinated mice could
334 only lead to T cell activation in the presence of BMDCs from hCD1Tg mice (**Fig 6**).

335 We demonstrated MA persistence in the lung 6 weeks post-vaccination using an *in vivo* antigen
336 presentation assay with adoptive transfer of naïve MA-specific T cells. Sustained release of antigen
337 through vaccination is thought to be key in the development of a robust adaptive immune response [56,
338 57]. Recently, spike protein was found within the draining lymph nodes of vaccinated human subjects
339 60 days after COVID-19 vaccination with mRNA-1273 or BNT162b2 [58]. In mice, pulmonary
340 vaccination with adenovirus expressing influenza nucleoprotein supported long term maintenance of
341 CD8 T_{RM} (resident memory) cells [59]. Unlike in this work, antigen persistence did not occur after
342 subcutaneous vaccination, suggesting a distinct mechanism of antigen archiving. In a different vaccine
343 model, subcutaneous administration of ovalbumin paired with adjuvants polyI:C and anti-CD40 led to
344 antigen archiving by LECs [11, 12]. Similar to our findings, antigen-specific T cell activation required
345 cross-presentation by DCs [11, 60]. Both LECs and FDCs retain antigens within a non-degradative
346 compartment [11, 61], suggesting that residual antigens in our model may similarly remain in the
347 endosome within undigested BCN. We have previously demonstrated the enhanced stability of BCN
348 within cell endosomes *in vitro* for extensive periods of time [22]. This possibility is corroborated by
349 the finding that DiD, which is easily quenched in aqueous solution [36], remained fluorescent 6 weeks
350 post-vaccination (**Fig 6**). The lack of persistence for Ag85B could be due to its leakage out from the
351 aqueous pores of BCN, which we have observed for other proteins [29]. Peptide antigens may be
352 modified to include a hydrophobic tail for stable retention within BCN and therefore allow for peptide
353 antigen persistence as well. MA's extreme hydrophobic surface, which correlates with its low
354 permeability as a part of Mtb cell wall, may also contribute to its prolonged persistence *in vivo* [62].

355 After infection and vaccination, peptide antigen persistence has been shown to occur through
356 archiving by binding to CD21 receptors on follicular dendritic cells (FDCs) in lymph nodes [3, 4]. MA

357 antigen persistence may likewise be a natural phenomenon that can occur after infections, although its
358 detection may be difficult given the lack of available assays to detect very small amounts of lipid
359 antigen. T cells may, in fact, be more sensitive than any commercially available tool. While we
360 determined that MA persists within AMs following pulmonary vaccination, this localization is likely
361 dependent on the vaccination route. In the case of SC and IV routes, significant exposure of AMs to
362 MA-BCN is unlikely to occur. Consequently, the exact localization of MA after vaccination via SC,
363 IV, or attenuated Mtb remains to be determined, and it is plausible that other types of macrophages
364 may be involved in this process. Additionally, we found that different forms of encapsulation (such as
365 BCN, MC, attenuate Mtb) can induce antigen persistence, DC internalization alone was not sufficient
366 to replicate this phenomenon (**Fig 5**). Thus, the question still remains regarding the necessary
367 properties of the delivery vector for the persistence of antigens to occur. Overall, MA antigen
368 persistence is a robust phenomenon which occurs independently of the vector and vaccine route of
369 administration, and thus may play a role in the efficacy of a variety of vaccine strategies. Additional
370 work will focus on whether lipid antigen persistence is found across the lipid family or specific to
371 lipids with certain properties.

372 Antigen persistence can also occur in chronic infections in which it is known to induce T cell
373 exhaustion [63]. Despite differentiating in an environment of persistent antigen exposure, memory
374 DN1 T cells exhibited a gene expression profile more similar to that of Tfh cells rather than exhausted
375 T cells (**Fig 7**). In particular, memory DN1 T cells upregulated the expression of TCF7 and BCL6
376 which are known to sustain a non-exhausted phenotype in CD8 T cells during chronic viral infections
377 [64, 65]. Previous studies on antigen archiving have suggested that the mere persistence of antigen is
378 insufficient for exhaustion to develop, and the inflammatory context likely plays a role in T cell
379 differentiation [11]. In many subunit vaccines, virulence factors are used as antigens to target and
380 suppress the pathogen's capacity to infect the host. The persistence of lipid virulence factors could
381 raise concerns regarding the safety of lipid vaccines. However, it is worth noting that otherwise toxic
382 compounds such as the lipid TDM have been successfully incorporated into numerous vaccines
383 without any known safety concerns to date [66-71]. The absence of reported safety issues may be

384 attributed to limited research or the administration of low doses of TDM. It is important to highlight
385 that while MA play a role in immune evasion, MA without additional functional groups has not been
386 shown to elicit similar toxic effects as TDM [62].

387 The use of memory T cells in the setting of antigen persistence may be debatable, given that
388 memory response has historically referred to the adaptive immune response in the setting of antigen
389 clearance [72]. However, given that the persistence of MA occurs even in the setting of attenuated Mtb
390 vaccination, Mtb lipid-specific long-term adaptive immunity will likely naturally exist in an antigen
391 persistent environment. We found that DN1 T cells in this setting expressed key markers of Tfh cells
392 such as CXCR5, PD-1, BCL6, and TCF1 (**Fig 7**). T cells differentiate into Tfh cells through the
393 expression of master transcription factor regulator BCL6, which directs the upregulation of chemokine
394 receptors CXCR5 and CXCR4 and thus migration into the germinal center[73, 74]. In the germinal
395 center, Tfh cells provide help to B cells for affinity maturation and class switching. Other
396 unconventional T cells are known to behave similarly such as CD1d-restricted NKT cells, which can
397 acquire a Tfh phenotype and provide B cell help through both cognate and non-cognate
398 interactions[75]. Additional work will look at whether DN1 or other group 1 CD1-restricted T cells can
399 functionally act as Tfh cells to provide B cell help, as may be suggested by the existence of IgG
400 antibodies against MA and glycolipid lipoarabinomannan in TB patients [76-78].

401 While persistence of protein antigen has been shown to improve the quality of protective
402 immunity [7, 11, 79, 80], it is not yet known how lipid antigen persistence may affect the protective
403 efficacy of lipid-specific T cells. At the very least, antigen persistence increases the probability of T
404 cell/DC encounters by increasing the time that the antigen is available. Additional work will need to
405 address the function of lipid-specific T cells differentiated in antigen persistent environments. As the
406 ultimate goal of this work is to improve the efficacy of existing subunit vaccines, future work will
407 assess the protective capacity of lipid antigen vaccines paired with additional protein antigens and
408 adjuvants.

409 ## Materials and Methods

410

411 **Ethics statement**

412 This study was carried out in accordance with the recommendations in the Guide for the Care and Use
413 of Laboratory Animals of the National Institutes of Health. The protocol was approved by the
414 Institutional Animal Care and Use Committee of Northwestern University (Protocol number:
415 IS000011717).

416

417 **Poly (ethylene glycol)-block-poly (propylene sulfide) polymer synthesis**

418 Poly (ethylene glycol)$_{17}$-block-poly-(propylene sulfide)$_{75}$ (PEG$_{17}$-*b*-PPS$_{75}$) copolymer was synthesized
419 as previously reported [81, 82]. Briefly, monomethoxy PEG (molecular weight=750 Da) was
420 functionalized with mesyl chloride and substituted with thioacetate to produce a PEG acetate initiator
421 for the polymerization for PPS.

422

423 **Bicontinuous nanosphere fabrication via flash nano precipitation**

424 BCN were produced using FNP technique as previously described[81]. In brief, PEG$_{17}$-*b*-PPS$_{75}$ BCN
425 polymer and any hydrophobic cargo was dissolved in THF and loaded onto a syringe. The hydrophilic
426 cargo was loaded onto a separate syringe, and both impinged against one another through the confined
427 impingement mixer into scintillation vial. The vial was placed in a vacuum desiccator overnight to
428 remove the organic solvent. NPs were filtered through LH-20 column with PBS as an eluent and
429 suspended in PBS for later use. A natural mixture of Mtb MA consists of α-, keto-, and methoxy forms
430 of MA with chain lengths of 72-86 carbon atom was obtained from Sigma (M4537, Sigma-Aldrich, St.
431 Louis, MO) [83]. MA encapsulation efficiency was analyzed using coumarin derivatization as
432 previously described [21]. MA was loaded at a concentration of 100 µg/mL of total BCN formulation
433 and DiD was loaded at 5 µg/mL total BCN formulation. MA loading capacity in BCNs was 2%. To
434 measure the encapsulation efficiency of Ag85B, Ag85B-MA-BCN were centrifuged at 10,000 g for 10
435 minutes. The supernatant was collected and concentrated using Amicon® Ultra-4 10K centrifugal filter

436 devices. To determine the unencapsulated protein concentration, the supernatant was incubated with
437 Pierce™ BCA Protein assay reagent following the manufacturer protocol and the absorbance was
438 measured at 660 nm using a SpectraMax M3 multi-mode microplate reader (Molecular Devices, LLC).
439 The percentage encapsulation efficiency was calculated as a percent of encapsulated protein to the total
440 amount of protein added. Ag85B was encapsulated at a concentration of 140 µg/mL and loading
441 capacity was found to be 2.88%.
442
443 **Poly (lactic-co-glycolic acid nanoparticle (NP) fabrication**
444 PLGA-NP were prepared by the Oil-in-Water single emulsion method. Briefly, PLGA (20 mg in 800
445 µL dichloromethane) organic phase was emulsified using an ultrasonic processor with aqueous phase
446 containing 2 mL of polyvinyl alcohol (PVA) solution (2.5% w/v) to form an emulsion. The emulsion
447 was then added dropwise into 4 mL of stirring 0.5% w/v PVA solution at room temperature to
448 evaporate the organic solvent. NPs were collected after 4 hours of stirring followed by centrifugation at
449 10,000 x g for 10 minutes. After centrifugation, NPs were washed twice with cold water to remove
450 residual PVA and redispersed in PBS. Hydrophilic (Texas red-Dextran) or hydrophobic (MA) loading
451 was performed by adding the payloads to the aqueous and organic phases, respectively.
452
453 **Nanocarrier characterization**
454 The nanocarrier size (z-average diameter) and polydispersity was measured using dynamic light
455 scattering (DLS) using a Nano 300 ZS Zetasizer (Malvern Panalytical, Malvern, U.K.). BCN and
456 PLGA morphology was visualized with cryogenic transmission electron microscopy (cryoTEM) as
457 previously detailed [21]. Transmission electron microscopy (TEM) was performed to image BCN
458 using uranyl acetate as a negative stain as previously reported [22]. BCN aggregate structure and
459 internal morphology was characterized with small angle X-ray scattering (SAXS). These studies were
460 performed at the DuPont-Northwestern-Dow Collaborative Access Team beamline at Argonne
461 National Laboratory's Advanced Photon Source with 10 keV (wavelength $\lambda = 1.24$ Å) collimated X-
462 rays, as described previously[81].
463

464 **Confocal imaging**

465 Confocal images of RAW 264.7 macrophages stained with lysosomal dye Lysotracker™ (green) and
466 NucBlue™ stain (blue) following incubation with Texas Red-labeled PLGA-NP and BCN (red) for 8
467 hr. The cells were then imaged within a humidified chamber using a 63X oil-immersion objective on a
468 SP5 Leica Confocal Microscope using HyD detectors and lasers. Data analysis was performed using
469 ImageJ software.

470

471 **Mouse strains**

472 Human CD1 transgenic mice (hCD1Tg) in C57BL/6 background or MHC II-deficient background [19]
473 and CD1b-restricted MA-specific TCR transgenic mice on $Rag^{-/-}$ background (DN1Tg/hCD1Tg/$Rag^{-/-}$)
474 [20] were generated in our lab as previously described. P25-specific TCR transgenic mice (Jackson
475 lab) were crossed onto $Rag^{-/-}$ background. Both males and females were used.

476

477 **Antibodies and flow cytometry**

478 For cell surface staining, cells were pre-incubated with 2.4G2 Fcγ RII/RIII blocking mAb for 15
479 minutes and then stained with the appropriate combinations of mAbs diluted in HBSS + 2% FBS for
480 30 minutes at 4ºC. Cells were analyzed on a BD FACS CantoII, or Cytek Aurora Spectral Cytometer
481 and data were processed with FlowJo software (TreeStar). The complete list of antibodies use is as
482 follows: anti-human Vβ5.1 (LC4, Invitrogen), anti-TCRβ (H57-597, BioLegend), anti-CD44 (IM7,
483 BioLegend), anti-Vβ11 (KT11, BioLegend), anti-CD45.2 (104, BioLegend), anti-CD45.1 (A20,
484 BioLegend), anti-SiglecF (E50-2440, BD Bioscience), anti-CD45 (30-F11, BioLegend), anti-CD11c
485 (N418, BioLegend), anti-CD11b (M1/70, BioLegend), anti-Ly6G (1A8, BioLegend), anti-CD19 (6D5,
486 BioLegend), anti-NK1.1 (PK136, BioLegend), anti-CD3 (17A2, BioLegend), Zombie Red
487 (BioLegend), anti-mouse CD185/CXCR5 (L138D7, Biolegend), anti-mouse CD279/PD-1 (29F.1A12,
488 Biolegend), and anti-Ki67 (SolA15, Invitrogen).

489

490 ***In vitro* nanoparticle and lipid titration with MA-specific DN1 T cells**

491 Nanoparticle and lipid titrations were performed as previously described [21]. In brief, hCD1Tg MHC
492 II$^{-/-}$ bone marrow-derived dendritic cells (BMDCs) were pulsed with varying quantities of nanoparticle
493 of sonicated MA and then co-cultured for 48 hours with DN1 T cells isolated from lymph nodes (axial,
494 brachial, submandibular, inguinal) of DN1Tg/hCD1Tg/Rag$^{-/-}$ mice. The supernatant was used for IFN-
495 γ enzyme-linked immunosorbent assay (ELISA) performed as described previously [21] and cells were
496 stained for activation.
497
498 ***In vitro* nanoparticle and lipid titration with human cells via ELISPOT assay**
499 Hydrophobic polyvinylidene fluoride 96-well plates (Millipore, Bedford, MA) were coated with anti-
500 human IFN-γ mAb 1-D1K (Mabtech, Cincinnati, OH) diluted 1:400 in PBS (Gibco, Waltham, MA)
501 and incubated at 4°C overnight. The following day, mAb was removed and each plate was washed and
502 incubated at room temperature for 2 hours in the presence of media. Human monocyte-derived
503 dendritic cells and MA-specific M11 T cells were seeded 50,000 cells and 2,000 cells per well,
504 respectively, together with serially diluted MA and NPs. After 16-hour incubation, plates were washed
505 and incubated with biotinylated anti-human IFN-g (7-B6-1), diluted 1:3000 in PBS + 0.5% FBS, for 4
506 hours. Plates were then washed with PBS 5 times and incubated for 2 hours with ExtrAvidin-Alkaline
507 phosphatase diluted 1:1000 in PBS + 0.5% FBS. Spots were visualized after incubation with the
508 BCIP/NBT substrate for up to 20 minutes and then imaged with ImmunoSpot reader v.2.0.
509
510 **Mouse vaccination**
511 For both intranasal (IN) and intratracheal (IT) vaccination, mice were anesthetized using inhaled
512 isoflurane. For IN vaccination, 25 μL of liquid was administered at the nostrils of the mice for a total
513 of 1 μg of MA per mouse. For IT vaccination, mice were administered 25 or 50 μL of liquid for a total
514 of 2.5 μg of MA with or without 2.0 μg of Ag85B. For BMDC vaccinations, hCD1Tg BMDCs were
515 cultured in GM-CSF and IL-4 for 5 days[84] and pulsed with MA-BCN (5 μg/mL of MA) or free MA
516 (10 μg/mL of MA) for 24 hours. Cells were washed and resuspended in PBS and IT vaccinated at a
517 dose of $1x10^6$ BMDCs/mouse. Intravenous vaccination was administered by tail vein injection.
518 Subcutaneous vaccination was administered between the shoulders over the neck portion of the mouse.

519

520 **Vaccination with attenuated Mtb**

521 Attenuated Mtb strain (H37Rv Δ*panCD* Δl*euCD* referred to as mc^2 6206) was kindly provided by
522 Jacobs' Laboratory at Albert Einstein College of Medicine. Bacteria were grown as previously
523 described in supplemented Middlebrook 7H9 media [35, 85]. Mice were vaccinated subcutaneously
524 with $1x10^6$ CFU in 100 µL of PBS. Mycobacterial burden quantification was performed by plating
525 serial dilutions of lung or spleen homogenate on Middlebrook 7H11 agar plates [35, 85].

526

527 **T cell Adoptive transfer and cell preparation**

528 DN1 or p25 T cells were isolated from lymph nodes of DN1Tg/hCD1Tg/$Rag^{-/-}$ or P25Tg/$Rag^{-/-}$ mice,
529 respectively. Cells were labeled with CellTrace™ Violet reagent (Invitrogen™) as per manufacturer's
530 instructions and $3\text{-}5x10^6$ cells were injected into hCD1Tg mice either 1 day before vaccination (short
531 term) or 6 weeks post-vaccination (long term). On day 7 post-adoptive transfer, draining lymph nodes
532 (axial, brachial, mediastinal), lung, and spleen were obtained. Single-cell suspensions were prepared
533 by mechanical disruption in HBSS/2% FBS. The lung was digested with collagenase IV (1mg/ml;
534 Sigma-Aldrich) and DNase I (30µg/ml; Sigma- Aldrich) for 30 minutes at 37ºC before the disruption.

535

536 **Biodistribution imaging**

537 BCN were loaded with DiD dye (Thermo Fisher) and administered to mice IT at 4 hours, 24 hours, 48
538 hours, 6 days, and 6 weeks prior to the final time point, at which all mice were sacrificed and analyzed
539 together. Lung, spleen, and draining lymph nodes were harvested and imaged using a near-IR *in vivo*
540 Imaging System (IVIS; Center for Advanced Molecular Imaging, Northwestern University). The
541 single-cell suspension was then prepared from indicated organs and cells were stained for flow
542 cytometric analysis.

543

544 **Alveolar macrophage enrichment and T cell co-culture**

545 hCD1Tg mice were immunized IT with either BCN or MA-BCN (2.5 µg of MA/mouse). 6 weeks
546 later, lungs were isolated and single-cell suspension was stained with anti-SiglecF-PE (E50-2440, BD

547 Bioscience). SiglecF-positive cells were enriched using anti-PE MultiSort Kit (Miltenyi Biotec). $1x10^5$
548 flow through and AM enriched fractions were co-cultured with $1x10^5$ hCD1Tg BMDCs and $3x10^5$
549 DN1 T cells for 48 hours and cells were stained for the expression of activation markers.
550
551 **Generation and vaccination of BM chimeras**
552 Bone marrow cells ^{from} DN1Tg/hCD1Tg/Rag$^{-/-}$ (CD45.2) and hCD1Tg mice (CD45.1) were depleted of
553 mature T cells using anti-Thy-1.2 (AT83.A-6) plus rabbit complement (Cedarlane Laboratories). Equal
554 numbers of cells ($5x10^6$) were adoptively transferred into hCD1Tg (CD45.1) mice irradiated with 900
555 rads. After 6 weeks, BM chimeric mice were intratracheally vaccinated with either 2.5 μg of MA in
556 MA-BCN or equivalent volume of PBS and the activation status of DN1 T cells were monitored in the
557 blood 1-2 times per week until experiment completion.
558
559 **RNA-Seq analysis**
560 CD44$^+$CD62L$^+$ and CD44$^-$CD62L$^+$ DN1 T cells were sorted from LNs of DN1-hCD1Tg BM chimera
561 mice vaccinated with MA-BCN at 6 weeks post vaccination by BD FACS Aria with purity >98%.
562 RNA was extracted with RNAeasy® mini kit (Qiagen). Libraries were generated by using the Illumina
563 Truseq preparation kit and sequenced on HiSeq4000. Reads were analyzed with Ceto pipeline
564 (https://github.com/ebartom/NGSbartom) using STAR and HTseq for alignment on mm10 mouse
565 genome and reading counting, as described previously [86]. Paired differential expression analysis was
566 performed using DESeq2 to account for original mouse sourcing[87]. All downstream analysis was
567 performed in R and figured generated using ggplot. Gene enrichment analysis was performed using
568 Metascape [88]. Comparisons to other T cell profiles were performed using raw transcriptome data
569 from ImmGen database[89], and two additional publications for follicular helper (T_{FH})[90], exhausted
570 (Texh)[91]. Analysis was performed as described above to obtain gene expression fold change values
571 relative to internal naïve condition.
572
573 **Data accessibility**

The data discussed in this publication have been deposited in NCBI's Gene Expression Omnibus and are accessible through GEO Series accession number GSE226075 (https://www.ncbi.nlm.nih.gov/geo/query/acc.cgi?acc=GSE226075).

Statistical analysis

Statistical analyses were performed using Prism software 9 (GraphPad software, Inc.). Multi-group comparisons were done using two-way analysis of variance (ANOVA) with significance determined by Tukey's multiple comparison. Where appropriate, outliers were identified through Grubbs method with alpha=0.05. Statistically significance denoted as ns = not significant, *$p<0.05$, **$p<0.01$, ***$p<0.001$, and ****$p< 0.0001$.

Acknowledgments

We thank Ying He for her support through maintaining laboratory reagents and equipment, Elizabeth Bartom for use of her RNASeq analysis pipeline, and Michael Kleyman for his advice on comparing gene expression among multiple T cell populations. We would like to thank the Center for Advanced Molecular Imaging (CAMI) for their help in performing IVIS and The Northwestern University's Atomic and Nanoscale Characterization Experimental Center (NUANCE) Keck-II facility for their help with NP characterization. Ag85B from *Mycobacterium tuberculosis* H37Rv was obtained through BEI Resources, NIAID, NIH. SAXS experiments were performed at the DuPont-Northwestern-Dow Collaborative Access Team (DND-CAT) located at Sector 5 of the Advanced Photon Source. DND-CAT is supported by Northwestern University, The Dow Chemical Company, and DuPont de Nemours, Inc. This research used resources of the Advanced Photon Source; a U.S. Department of Energy (DOE) Office of Science User Facility operated for the DOE Office of Science by Argonne National Laboratory under Contract No. DE-AC02-06CH11357. Data was collected using an instrument funded by the National Science Foundation under Award No. 0960140.

Funding:

This work was supported by the following grans:

National Institutes of Health grant R01AI057460 (CRW), R01AI145345 (CRW, EAS)
National Institutes of Health grant F30AI157314 (EM)
National Institutes of Health grant T32GM008152 (EM)
National Institutes of Health grant R01AI146072 (CS)

Competing interests: Authors declare that they have no competing financial interests.

Data and materials availability:

All data are available in the main text or the supplementary materials. Derived data supporting the findings of this study are available from the corresponding author CRW and EAS on request. Generated transgenic mice and nanoparticles are available upon request upon signing of Material Transfer Agreement (MTA).

Nonstandard Abbreviations:

Mtb, *Mycobacterium tuberculosis*; MA, mycolic acid; BCN, bicontinuous nanospheres; MA-BCN, mycolic acid loaded bicontinuous nanospheres; FDCs, follicular dendritic cells; LECs, lymphocytic endothelial cells; hCD1Tg, human CD1 transgenic mouse model; APCs, antigen-presenting cells; PEG-b-PPS, poly(ethylene glycol)-block-poly(propylene sulfide); MA-MC, mycolic acid loaded micellar nanocarrier; FNP, flash nanoprecipitation; PLGA, poly(D,L-lactide-co-glycolide); DLS, dynamic light scattering; PDI, polydispersity index; cryo-TEM, cryogenic transmission electron microscopy; SAXS, small angle X-ray scattering; PLGA-NP, poly(D,L-lactide-co-glycolide) nanoparticle; MA-PLGA, mycolic acid loaded poly(D,L-lactide-co-glycolide); IN, intranasal; IT, intratracheal; Ag85B-MA-BCN, Ag85B and mycolic acid loaded bicontinuous nanosphere; BMDCs, bone marrow-derived dendritic cells; DiD-BCN, DiD loaded bicontinuous nanosphere; AMs, alveolar macrophages.

628 **References**

629

630 1. Karch CP, Burkhard P. Vaccine technologies: From whole organisms to rationally designed
631 protein assemblies. Biochem Pharmacol. 2016;120:1-14. Epub 20160506. doi:
632 10.1016/j.bcp.2016.05.001. PubMed PMID: 27157411; PubMed Central PMCID: PMCPMC5079805.
633 2. Legoux F, Salou M, Lantz O. Unconventional or Preset alphabeta T Cells: Evolutionarily
634 Conserved Tissue-Resident T Cells Recognizing Nonpeptidic Ligands. Annu Rev Cell Dev Biol.
635 2017;33:511-35. Epub 20170629. doi: 10.1146/annurev-cellbio-100616-060725. PubMed PMID:
636 28661722.
637 3. Heesters BA, Myers RC, Carroll MC. Follicular dendritic cells: Dynamic antigen libraries.
638 Nature Publishing Group; 2014. p. 495-504.
639 4. Hirosue S, Dubrot J. Modes of antigen presentation by lymph node stromal cells and their
640 immunological implications. Frontiers in Immunology. 2015;6. doi: ARTN 446
641 10.3389/fimmu.2015.00446. PubMed PMID: WOS:000361632700001.
642 5. Takamura S, Roberts AD, Jelley-Gibbs DM, Wittmer ST, Kohlmeier JE, Woodland DL. The
643 route of priming influences the ability of respiratory virus-specific memory CD8+ T cells to be
644 activated by residual antigen. Journal of Experimental Medicine. 2010;207(6):1153-60. doi:
645 10.1084/jem.20090283.
646 6. Kim TS, Hufford MM, Sun J, Fu YX, Braciale TJ. Antigen persistence and the control of local
647 T cell memory by migrant respiratory dendritic cells after acute virus infection. Journal of
648 Experimental Medicine. 2010;207(6):1161-72. doi: 10.1084/jem.20092017.
649 7. Demento SL, Cui W, Criscione JM, Stern E, Tulipan J, Kaech SM, et al. Role of sustained
650 antigen release from nanoparticle vaccines in shaping the T cell memory phenotype. Biomaterials.
651 2012;33(19):4957-64. Epub 20120406. doi: 10.1016/j.biomaterials.2012.03.041. PubMed PMID:
652 22484047; PubMed Central PMCID: PMCPMC5724530.
653 8. Zammit DJ, Turner DL, Klonowski KD, Lefrançois L, Cauley LS. Residual Antigen
654 Presentation after Influenza Virus Infection Affects CD8 T Cell Activation and Migration. Immunity.
655 2006;24(4):439-49. doi: 10.1016/j.immuni.2006.01.015.

656 9. Woodland DL, Kohlmeier JE. Migration, maintenance and recall of memory T cells in
657 peripheral tissues. Nat Rev Immunol. 2009;9(3):153-61. doi: 10.1038/nri2496. PubMed PMID:
658 19240755.
659 10. Vokali E, Yu SS, Hirosue S, Rincon-Restrepo M, F VD, Scherer S, et al. Lymphatic endothelial
660 cells prime naive CD8(+) T cells into memory cells under steady-state conditions. Nat Commun.
661 2020;11(1):538. Epub 20200127. doi: 10.1038/s41467-019-14127-9. PubMed PMID: 31988323;
662 PubMed Central PMCID: PMCPMC6985113.
663 11. Tamburini BA, Burchill MA, Kedl RM. Antigen capture and archiving by lymphatic
664 endothelial cells following vaccination or viral infection. Nature Communications. 2014;5(1):3989-.
665 doi: 10.1038/ncomms4989.
666 12. Walsh SM, Sheridan RM, Lucas ED, Doan TA, Ware BC, Schafer J, et al. Molecular tracking
667 devices quantify antigen distribution and archiving in the murine lymph node. Elife. 2021;10. Epub
668 20210412. doi: 10.7554/eLife.62781. PubMed PMID: 33843587; PubMed Central PMCID:
669 PMCPMC8116055.
670 13. Reinink P, Van Rhijn I. Mammalian CD1 and MR1 genes. Immunogenetics. 2016;68(8):515-
671 23. Epub 20160728. doi: 10.1007/s00251-016-0926-x. PubMed PMID: 27470004; PubMed Central
672 PMCID: PMCPMC5002277.
673 14. Joosten SA, Ottenhoff THM, Lewinsohn DM, Hoft DF, Moody DB, Seshadri C. Harnessing
674 donor unrestricted T-cells for new vaccines against tuberculosis. 2019. p. 3022-30.
675 15. Morgun E, Cao LC, Wang C-R. Role of Group 1 CD1-restricted T Cells in Host Defense and
676 Inflammatory Diseases. Critical Reviews in Immunology. 2021. doi:
677 10.1615/critrevimmunol.2021040089.
678 16. Busch M, Herzmann C, Kallert S, Zimmermann A, Hofer C, Mayer D, et al.
679 Lipoarabinomannan-responsive polycytotoxic T cells are associated with protection in human
680 tuberculosis. American Journal of Respiratory and Critical Care Medicine. 2016;194(3):345-55. doi:
681 10.1164/rccm.201509-1746OC.

682 17. Lopez K, Iwany SK, Suliman S, Reijneveld JF, Ocampo TA, Jimenez J, et al. CD1b Tetramers
683 Broadly Detect T Cells That Correlate With Mycobacterial Exposure but Not Tuberculosis Disease
684 State. Frontiers in Immunology. 2020;11:199-. doi: 10.3389/fimmu.2020.00199.
685 18. Montamat-Sicotte DJ, Millington KA, Willcox CR, Hingley-Wilson S, Hackforth S, Innes J, et
686 al. A mycolic acid-specific CD1-restricted T cell population contributes to acute and memory immune
687 responses in human tuberculosis infection. Journal of Clinical Investigation. 2011;121(6):2493-503.
688 doi: 10.1172/JCI46216.
689 19. Felio K, Nguyen H, Dascher CC, Choi H-J, Li S, Zimmer MI, et al. CD1-restricted adaptive
690 immune responses to Mycobacteria in human group 1 CD1 transgenic mice. The Journal of
691 experimental medicine. 2009;206(11):2497-509. doi: 10.1084/jem.20090898.
692 20. Zhao J, Siddiqui S, Shang S, Bian Y, Bagchi S, He Y, et al. Mycolic acid-specific T cells
693 protect against Mycobacterium tuberculosis infection in a humanized transgenic mouse model. eLife.
694 2015;4. doi: 10.7554/eLife.08525.
695 21. Shang S, Kats D, Cao L, Morgun E, Velluto D, He Y, et al. Induction of Mycobacterium
696 Tuberculosis Lipid-Specific T Cell Responses by Pulmonary Delivery of Mycolic Acid-Loaded
697 Polymeric Micellar Nanocarriers. Frontiers in Immunology. 2018;9:2709-. doi:
698 10.3389/fimmu.2018.02709.
699 22. Bobbala S, Allen SD, Yi S, Vincent M, Frey M, Karabin NB, et al. Employing bicontinuous-to-
700 micellar transitions in nanostructure morphology for on-demand photo-oxidation responsive cytosolic
701 delivery and off-on cytotoxicity. Nanoscale. 2020;12(9):5332-40. doi: 10.1039/c9nr10921h.
702 23. Burke JA, Zhang X, Bobbala S, Frey MA, Bohorquez Fuentes C, Freire Haddad H, et al.
703 Subcutaneous nanotherapy repurposes the immunosuppressive mechanism of rapamycin to enhance
704 allogeneic islet graft viability. Nat Nanotechnol. 2022. Epub 20220117. doi: 10.1038/s41565-021-
705 01048-2. PubMed PMID: 35039683.
706 24. Du F, Liu YG, Scott EA. Immunotheranostic Polymersomes Modularly Assembled from
707 Tetrablock and Diblock Copolymers with Oxidation-Responsive Fluorescence. Cell Mol Bioeng.
708 2017;10(5):357-70. Epub 20170410. doi: 10.1007/s12195-017-0486-7. PubMed PMID: 28989540;
709 PubMed Central PMCID: PMCPMC5628512.

710 25. Scott EA, Stano A, Gillard M, Maio-Liu AC, Swartz MA, Hubbell JA. Dendritic cell activation
711 and T cell priming with adjuvant- and antigen-loaded oxidation-sensitive polymersomes. Biomaterials.
712 2012;33(26):6211-9. doi: 10.1016/j.biomaterials.2012.04.060.
713 26. Napoli A, Valentini M, Tirelli N, Müller M, Hubbell JA. Oxidation-responsive polymeric
714 vesicles. Nature Materials. 2004;3(3):183-9. doi: 10.1038/nmat1081.
715 27. Allen SD, Bobbala S, Karabin NB, Scott EA. On the advancement of polymeric bicontinuous
716 nanospheres toward biomedical applications. Nanoscale Horiz. 2019;4(2):258-72. Epub 20181120.
717 doi: 10.1039/c8nh00300a. PubMed PMID: 32254084.
718 28. Saad WS, Prud'Homme RK. Principles of nanoparticle formation by flash nanoprecipitation.
719 Nano Today. 2016;11(2):212-27. doi: 10.1016/j.nantod.2016.04.006.
720 29. Bobbala S, Allen SD, Scott EA. Flash nanoprecipitation permits versatile assembly and loading
721 of polymeric bicontinuous cubic nanospheres. Nanoscale. 2018;10(11):5078-88. doi:
722 10.1039/C7NR06779H.
723 30. Lin LCW, Chattopadhyay S, Lin JC, Hu CMJ. Advances and Opportunities in Nanoparticle-
724 and Nanomaterial-Based Vaccines against Bacterial Infections. Wiley-Blackwell; 2018. p. 1701395-.
725 31. Khademi F, Derakhshan M, Yousefi-Avarvand A, Tafaghodi M. Potential of polymeric
726 particles as future vaccine delivery systems/adjuvants for parenteral and non-parenteral immunization
727 against tuberculosis: A systematic review. Mashhad University of Medical Sciences; 2018. p. 116-23.
728 32. Modak M, Bobbala S, Lescott C, Liu YG, Nandwana V, Dravid VP, et al. Magnetic
729 Nanostructure-Loaded Bicontinuous Nanospheres Support Multicargo Intracellular Delivery and
730 Oxidation-Responsive Morphological Transitions. ACS Appl Mater Interfaces. 2020;12(50):55584-95.
731 Epub 20201201. doi: 10.1021/acsami.0c15920. PubMed PMID: 33259182.
732 33. Huygen K. The Immunodominant T-Cell Epitopes of the Mycolyl-Transferases of the Antigen
733 85 Complex of M. tuberculosis. Front Immunol. 2014;5:321. Epub 20140709. doi:
734 10.3389/fimmu.2014.00321. PubMed PMID: 25071781; PubMed Central PMCID: PMCPMC4089088.
735 34. Tamura T, Ariga H, Kinashi T, Uehara S, Kikuchi T, Nakada M, et al. The role of antigenic
736 peptide in CD4+ T helper phenotype development in a T cell receptor transgenic model. International
737 Immunology. 2004;16(12):1691-9. doi: 10.1093/intimm/dxh170.

738 35. Sampson SL, Dascher CC, Sambandamurthy VK, Russell RG, Jacobs WR, Jr., Bloom BR, et
739 al. Protection elicited by a double leucine and pantothenate auxotroph of Mycobacterium tuberculosis
740 in guinea pigs. Infect Immun. 2004;72(5):3031-7. doi: 10.1128/IAI.72.5.3031-3037.2004. PubMed
741 PMID: 15102816; PubMed Central PMCID: PMCPMC387862.
742 36. Invitrogen™. DiD' solid; DiIC18(5) solid (1,1'-Dioctadecyl-3,3,3',3'-
743 Tetramethylindodicarbocyanine, 4-Chlorobenzenesulfonate Salt).
744 37. Barral DC, Brenner MB. CD1 antigen presentation: how it works. Nature Reviews
745 Immunology. 2007;7(12):929-41. doi: 10.1038/nri2191.
746 38. Dascher CC, Hiromatsu K, Xiong X, Morehouse C, Watts G, Liu G, et al. Immunization with a
747 mycobacterial lipid vaccine improves pulmonary pathology in the guinea pig model of tuberculosis.
748 Oxford University Press; 2003. p. 915-25.
749 39. Larrouy-Maumus G, Layre E, Clark S, Prandi J, Rayner E, Lepore M, et al. Protective efficacy
750 of a lipid antigen vaccine in a guinea pig model of tuberculosis. Vaccine. 2017;35(10):1395-402. doi:
751 10.1016/J.VACCINE.2017.01.079.
752 40. Eckhardt E, Bastian M. Animal models for human group 1 CD1 protein function. Molecular
753 Immunology. 2021;130:159-63. doi: 10.1016/j.molimm.2020.12.018.
754 41. Schrager LK, Vekemens J, Drager N, Lewinsohn DM, Olesen OF. The status of tuberculosis
755 vaccine development. Lancet Infect Dis. 2020;20(3):e28-e37. Epub 20200131. doi: 10.1016/S1473-
756 3099(19)30625-5. PubMed PMID: 32014117.
757 42. Wang Y, Qin B, Xia G, Choi SH. FDA's Poly (Lactic-Co-Glycolic Acid) Research Program
758 and Regulatory Outcomes. Aaps J. 2021;23(4):92. Epub 20210629. doi: 10.1208/s12248-021-00611-y.
759 PubMed PMID: 34189655.
760 43. Ding D, Zhu Q. Recent advances of PLGA micro/nanoparticles for the delivery of
761 biomacromolecular therapeutics. Materials Science & ENgineering C. 2018. doi:
762 10.1016/j.msec.2017.12.036.
763 44. Barillet S, Fattal E, Mura S, Tsapis N, Pallardy M, Hillaireau H, et al. Immunotoxicity of poly
764 (lactic-co-glycolic acid) nanoparticles: influence of surface properties on dendritic cell activation.

765 Nanotoxicology. 2019;13(5):606-22. Epub 20190214. doi: 10.1080/17435390.2018.1564078. PubMed
766 PMID: 30760076.
767 45. Ma S, Feng X, Liu F, Wang B, Zhang H, Niu X. The pro-inflammatory response of
768 macrophages regulated by acid degradation products of poly(lactide-co-glycolide) nanoparticles. Eng
769 Life Sci. 2021;21(10):709-20. Epub 20210512. doi: 10.1002/elsc.202100040. PubMed PMID:
770 34690640; PubMed Central PMCID: PMCPMC8518582.
771 46. Nicolete R, dos Santos DF, Faccioli LH. The uptake of PLGA micro or nanoparticles by
772 macrophages provokes distinct in vitro inflammatory response. Int Immunopharmacol.
773 2011;11(10):1557-63. Epub 20110527. doi: 10.1016/j.intimp.2011.05.014. PubMed PMID: 21621649.
774 47. Stylianou E, Paul MJ, Reljic R, McShane H. Mucosal delivery of tuberculosis vaccines: a
775 review of current approaches and challenges. Expert Rev Vaccines. 2019;18(12):1271-84. Epub
776 20191226. doi: 10.1080/14760584.2019.1692657. PubMed PMID: 31876199; PubMed Central
777 PMCID: PMCPMC6961305.
778 48. Ballester M, Nembrini C, Dhar N, de Titta A, de Piano C, Pasquier M, et al. Nanoparticle
779 conjugation and pulmonary delivery enhance the protective efficacy of Ag85B and CpG against
780 tuberculosis. Vaccine. 2011;29(40):6959-66. doi: 10.1016/j.vaccine.2011.07.039. PubMed PMID:
781 WOS:000295300500018.
782 49. Fels AO, Cohn ZA. The alveolar macrophage. J Appl Physiol (1985). 1986;60(2):353-69. doi:
783 10.1152/jappl.1986.60.2.353. PubMed PMID: 3005225.
784 50. Bowden DH. The alveolar macrophage. Environ Health Perspect. 1984;55:327-41. doi:
785 10.1289/ehp.8455327. PubMed PMID: 6376105; PubMed Central PMCID: PMCPMC1568378.
786 51. Geiser M. Update on macrophage clearance of inhaled micro- and nanoparticles. J Aerosol
787 Med Pulm Drug Deliv. 2010;23(4):207-17. doi: 10.1089/jamp.2009.0797. PubMed PMID: 20109124.
788 52. Pai M, Behr MA, Dowdy D, Dheda K, Divangahi M, Boehme CC, et al. Tuberculosis. Nat Rev
789 Dis Primers. 2016;2:16076. Epub 20161027. doi: 10.1038/nrdp.2016.76. PubMed PMID: 27784885.
790 53. Dougan SK, Kaser A, Blumberg RS. CD1 Expression on Antigen-Presenting Cells. 314. Berlin,
791 Heidelberg: Springer Berlin Heidelberg; 2007. p. 113-41.

792 54. Espinosa-Cueto P, Magallanes-Puebla A, Castellanos C, Mancilla R. Dendritic cells that
793 phagocytose apoptotic macrophages loaded with mycobacterial antigens activate CD8 T cells via
794 cross-presentation. PLoS One. 2017;12(8):e0182126. Epub 20170802. doi:
795 10.1371/journal.pone.0182126. PubMed PMID: 28767693; PubMed Central PMCID:
796 PMCPMC5540487.
797 55. Schaible UE, Winau F, Sieling PA, Fischer K, Collins HL, Hagens K, et al. Apoptosis
798 facilitates antigen presentation to T lymphocytes through MHC-I and CD1 in tuberculosis. Nat Med.
799 2003;9(8):1039-46. Epub 20030720. doi: 10.1038/nm906. PubMed PMID: 12872166.
800 56. Silva AL, Soema PC, Slutter B, Ossendorp F, Jiskoot W. PLGA particulate delivery systems
801 for subunit vaccines: Linking particle properties to immunogenicity. Hum Vaccin Immunother.
802 2016;12(4):1056-69. Epub 20160111. doi: 10.1080/21645515.2015.1117714. PubMed PMID:
803 26752261; PubMed Central PMCID: PMCPMC4962933.
804 57. Correia-Pinto JF, Csaba N, Alonso MJ. Vaccine delivery carriers: insights and future
805 perspectives. Int J Pharm. 2013;440(1):27-38. Epub 20120423. doi: 10.1016/j.ijpharm.2012.04.047.
806 PubMed PMID: 22561794.
807 58. Roltgen K, Nielsen SCA, Silva O, Younes SF, Zaslavsky M, Costales C, et al. Immune
808 imprinting, breadth of variant recognition, and germinal center response in human SARS-CoV-2
809 infection and vaccination. Cell. 2022;185(6):1025-40 e14. Epub 20220125. doi:
810 10.1016/j.cell.2022.01.018. PubMed PMID: 35148837; PubMed Central PMCID: PMCPMC8786601.
811 59. Uddback I, Cartwright EK, Scholler AS, Wein AN, Hayward SL, Lobby J, et al. Long-term
812 maintenance of lung resident memory T cells is mediated by persistent antigen. Mucosal Immunol.
813 2021;14(1):92-9. Epub 20200609. doi: 10.1038/s41385-020-0309-3. PubMed PMID: 32518368;
814 PubMed Central PMCID: PMCPMC7726002.
815 60. Kedl RM, Lindsay RS, Finlon JM, Lucas ED, Friedman RS, Tamburini BAJ. Migratory
816 dendritic cells acquire and present lymphatic endothelial cell-archived antigens during lymph node
817 contraction. Nat Commun. 2017;8(1):2034. Epub 20171211. doi: 10.1038/s41467-017-02247-z.
818 PubMed PMID: 29229919; PubMed Central PMCID: PMCPMC5725486.

819 61. Heesters BA, Chatterjee P, Kim YA, Gonzalez SF, Kuligowski MP, Kirchhausen T, et al.
820 Endocytosis and recycling of immune complexes by follicular dendritic cells enhances B cell antigen
821 binding and activation. Immunity. 2013;38(6):1164-75. Epub 20130613. doi:
822 10.1016/j.immuni.2013.02.023. PubMed PMID: 23770227; PubMed Central PMCID:
823 PMCPMC3773956.
824 62. Daffé M, Quémard A, Marrakchi H. Mycolic Acids: From Chemistry to Biology. 2019. p. 181-
825 216.
826 63. Barber DL, Wherry EJ, Masopust D, Zhu B, Allison JP, Sharpe AH, et al. Restoring function in
827 exhausted CD8 T cells during chronic viral infection. Nature. 2006;439(7077):682-7. doi:
828 10.1038/nature04444.
829 64. Wu T, Ji Y, Ashley Moseman E, Xu HC, Manglani M, Kirby M, et al. The TCF1-Bcl6 axis
830 counteracts type I interferon to repress exhaustion and maintain T cell stemness. Science Immunology.
831 2016;1(6). doi: 10.1126/sciimmunol.aai8593.
832 65. Wang Y, Hu J, Li Y, Xiao M, Wang H, Tian Q, et al. The transcription factor TCF1 preserves
833 the effector function of exhausted CD8 T cells during chronic viral infection. Frontiers in Immunology.
834 2019;10(FEB):169-. doi: 10.3389/fimmu.2019.00169.
835 66. Kwon KW, Kang TG, Lee A, Jin SM, Lim YT, Shin SJ, et al. Protective Efficacy and
836 Immunogenicity of Rv0351/Rv3628 Subunit Vaccine Formulated in Different Adjuvants Against
837 Mycobacterium tuberculosis Infection. Immune Netw. 2023;23(2):e16. Epub 20230216. doi:
838 10.4110/in.2023.23.e16. PubMed PMID: 37179749; PubMed Central PMCID: PMCPMC10166659.
839 67. Lima KM, Santos SA, Lima VM, Coelho-Castelo AA, Rodrigues JM, Jr., Silva CL. Single dose
840 of a vaccine based on DNA encoding mycobacterial hsp65 protein plus TDM-loaded PLGA
841 microspheres protects mice against a virulent strain of Mycobacterium tuberculosis. Gene Ther.
842 2003;10(8):678-85. doi: 10.1038/sj.gt.3301908. PubMed PMID: 12692596.
843 68. Niu H, Hu L, Li Q, Da Z, Wang B, Tang K, et al. Construction and evaluation of a multistage
844 Mycobacterium tuberculosis subunit vaccine candidate Mtb10.4-HspX. Vaccine. 2011;29(51):9451-8.
845 Epub 20111021. doi: 10.1016/j.vaccine.2011.10.032. PubMed PMID: 22024175.

846 69. Sarkar S, Mishra A, Periasamy S, Dyett B, Dogra P, Ball AS, et al. Prospective Subunit
847 Nanovaccine against Mycobacterium tuberculosis Infection horizontal line Cubosome Lipid
848 Nanocarriers of Cord Factor, Trehalose 6,6' Dimycolate. ACS Appl Mater Interfaces.
849 2023;15(23):27670-86. Epub 20230601. doi: 10.1021/acsami.3c04063. PubMed PMID: 37262346.
850 70. Welsh KJ, Hunter RL, Actor JK. Trehalose 6,6'-dimycolate--a coat to regulate tuberculosis
851 immunopathogenesis. Tuberculosis (Edinb). 2013;93 Suppl:S3-9. doi: 10.1016/S1472-9792(13)70003-
852 9. PubMed PMID: 24388646.
853 71. Xin Q, Niu H, Li Z, Zhang G, Hu L, Wang B, et al. Subunit vaccine consisting of multi-stage
854 antigens has high protective efficacy against Mycobacterium tuberculosis infection in mice. PLoS One.
855 2013;8(8):e72745. Epub 20130815. doi: 10.1371/journal.pone.0072745. PubMed PMID: 23967337;
856 PubMed Central PMCID: PMCPMC3744459.
857 72. Martin MD, Badovinac VP. Defining memory CD8 T cell. Frontiers Media SA; 2018.
858 73. Johnston RJ, Poholek AC, DiToro D, Yusuf I, Eto D, Barnett B, et al. Bcl6 and Blimp-1 are
859 reciprocal and antagonistic regulators of T follicular helper cell differentiation. Science.
860 2009;325(5943):1006-10. doi: 10.1126/science.1175870.
861 74. Nurieva RI, Chung Y, Martinez GJ, Yang XO, Tanaka S, Matskevitch TD, et al. Bcl6 mediates
862 the development of T follicular helper cells. Science. 2009;325(5943):1001-5. doi:
863 10.1126/science.1176676.
864 75. Clerici L, Casorati G, Dellabona P. B Cell Help by CD1d-Rectricted NKT Cells. Antibodies.
865 2015;4(4):279-94. doi: 10.3390/antib4040279.
866 76. Correia-Neves M, Sundling C, Cooper A, Kallenius G. Lipoarabinomannan in Active and
867 Passive Protection Against Tuberculosis. Front Immunol. 2019;10:1968. Epub 20190911. doi:
868 10.3389/fimmu.2019.01968. PubMed PMID: 31572351; PubMed Central PMCID: PMCPMC6749014.
869 77. Schleicher GK, Feldman C, Vermaak Y, Verschoor JA. Prevalence of anti-mycolic acid
870 antibodies in patients with pulmonary tuberculosis co-infected with HIV. Clinical Chemistry and
871 Laboratory Medicine. 2002;40(9):882-7. doi: 10.1515/CCLM.2002.156.

872 78. Pan J, Fujiwara N, Oka S, Maekura R, Ogura T, Yano I. Anti-cord factor (trehalose
873 6,6'dimycolate) IgG antibody in tuberculosis patients recognizes mycolic acid subclasses. Microbiol
874 Immunol. 1999;43(9):863-9. doi: 10.1111/j.1348-0421.1999.tb01221.x. PubMed PMID: 10553679.
875 79. Bioley G, Lassus A, Terrettaz J, Tranquart F, Corthésy B. Long-term persistence of immunity
876 induced by OVA-coupled gas-filled microbubble vaccination partially protects mice against infection
877 by OVA-expressing Listeria. Biomaterials. 2015;57:153-60. doi: 10.1016/j.biomaterials.2015.04.008.
878 80. Silva AL, Rosalia RA, Sazak A, Carstens MG, Ossendorp F, Oostendorp J, et al. Optimization
879 of encapsulation of a synthetic long peptide in PLGA nanoparticles: low-burst release is crucial for
880 efficient CD8(+) T cell activation. Eur J Pharm Biopharm. 2013;83(3):338-45. Epub 20121129. doi:
881 10.1016/j.ejpb.2012.11.006. PubMed PMID: 23201055.
882 81. Allen SD, Bobbala S, Karabin NB, Modak M, Scott EA. Benchmarking Bicontinuous
883 Nanospheres against Polymersomes for in Vivo Biodistribution and Dual Intracellular Delivery of
884 Lipophilic and Water-Soluble Payloads. ACS Applied Materials & Interfaces. 2018;10(40):33857-66.
885 doi: 10.1021/acsami.8b09906.
886 82. Frey M. Development and Optimization of Functionalized Self-Assembling Polymeric
887 Nanobiomaterials: Northwestern University; 2021.
888 83. Van Rhijn I, Iwany SK, Fodran P, Cheng TY, Gapin L, Minnaard AJ, et al. CD1b-mycolic acid
889 tetramers demonstrate T-cell fine specificity for mycobacterial lipid tails. European Journal of
890 Immunology. 2017;47(9):1525-34. doi: 10.1002/eji.201747062.
891 84. Li S, Choi HJ, Felio K, Wang CR. Autoreactive CD1b-restricted T cells: A new innate-like T-
892 cell population that contributes to immunity against infection. Blood. 2011;118(14):3870-8. doi:
893 10.1182/blood-2011-03-341941.
894 85. Larsen MH, Biermann K, Chen B, Hsu T, Sambandamurthy VK, Lackner AA, et al. Efficacy
895 and safety of live attenuated persistent and rapidly cleared Mycobacterium tuberculosis vaccine
896 candidates in non-human primates. Vaccine. 2009;27(34):4709-17. Epub 20090602. doi:
897 10.1016/j.vaccine.2009.05.050. PubMed PMID: 19500524; PubMed Central PMCID:
898 PMCPMC3512200.

899 86. Weng X, Kumar A, Cao L, He Y, Morgun E, Visvabharathy L, et al. Mitochondrial metabolism
900 is essential for invariant natural killer T cell development and function. Proc Natl Acad Sci U S A.
901 2021;118(13). Epub 2021/03/24. doi: 10.1073/pnas.2021385118. PubMed PMID: 33753493.
902 87. Love MI, Huber W, Anders S. Moderated estimation of fold change and dispersion for RNA-
903 seq data with DESeq2. Genome Biol. 2014;15(12):550. Epub 2014/12/18. doi: 10.1186/s13059-014-
904 0550-8. PubMed PMID: 25516281; PubMed Central PMCID: PMCPMC4302049.
905 88. Zhou Y, Zhou B, Pache L, Chang M, Khodabakhshi AH, Tanaseichuk O, et al. Metascape
906 provides a biologist-oriented resource for the analysis of systems-level datasets. Nature
907 Communications. 2019;10(1). doi: 10.1038/s41467-019-09234-6.
908 89. Yoshida H, Lareau CA, Ramirez RN, Rose SA, Maier B, Wroblewska A, et al. The cis-
909 Regulatory Atlas of the Mouse Immune System. Cell. 2019;176(4):897-912.e20. doi:
910 10.1016/j.cell.2018.12.036.
911 90. Lahmann A, Kuhrau J, Fuhrmann F, Heinrich F, Bauer L, Durek P, et al. Bach2 Controls T
912 Follicular Helper Cells by Direct Repression of Bcl-6. The Journal of Immunology. 2019;202(8):2229-
913 39. doi: 10.4049/jimmunol.1801400.
914 91. Man K, Gabriel SS, Liao Y, Gloury R, Preston S, Henstridge DC, et al. Transcription Factor
915 IRF4 Promotes CD8+ T Cell Exhaustion and Limits the Development of Memory-like T Cells during
916 Chronic Infection. Immunity. 2017;47(6):1129-41.e5. doi: 10.1016/j.immuni.2017.11.021.
917

918 **Figure Legends**

919

920 **Fig. 1. Physicochemical characterization of BCN and PLGA-NP. (A)** Dynamic light scattering
921 (DLS) analysis of blank BCN and MA-BCN. **(B)** CryoTEM of MA-BCN (scale = 500 nm). **(C)**
922 Negative staining TEM images of MA-BCN. **(D)** SAXS of blank BCN and MA-BCN. **(E)** DLS
923 analysis of blank PLGA and MA PLGA. **(F)** MA encapsulation efficiency for MA-BCN and MA
924 PLGA. N = 3 per condition. Data represented as mean ± SD.

925

926 **Fig. 2. MA-BCN effectively activated MA-specific T cells *in vitro* and *in vivo*. (A, B)** BMDCs were
927 pulsed for 18 hrs. with selected nanoparticles at various concentrations, co-cultured for 48 hrs. with
928 DN1 T cells, and T cell activation was measured. **(A)** Percentage of CD69 and CD25-expressing DN1
929 T cells. **(B)** IFN-g production measured by ELISA. (N=3). (**C, D**) ELISPOT of IFN-g from MA-
930 specific human M11 T cells cultured for 16 hours with monocyte-derived dendritic cells with selected
931 nanoparticles at high **(C)** and low **(D)** concentrations. Data are representative of two independent
932 experiments and displayed as mean ± SEM. Statistical analysis: 2-way ANOVA, significance
933 designated for MA-BCN vs free MA. (**E-G**) hCD1Tg mice were IN vaccinated with selected
934 nanoparticles and CellTrace Violet-labeled DN1 T cells were adoptively transferred the next day. After
935 1 week, DN1 T cell activation and proliferation was measured. **(E)** Representative FACS plots of DN1
936 T cells in the LN. Percentage of proliferating (**F**) and CD44-expressing **(G)** DN1 T cells in the LN and
937 lung. Data represented as mean ± SEM. Statistical analysis: 2-way ANOVA. *p<0.05, **p<0.01,
938 ***p<0.001, ****p< 0.0001.

939

940 **Fig. 3. Vaccination with MA-BCN leads to antigen persistence 6 weeks post-vaccination.** hCD1Tg
941 mice were IT vaccinated with MA-BCN or BCN. 6 weeks later, CellTrace-labeled p25 and DN1 T
942 cells were adoptively transferred, and T cell activation was measured after 1 week. **(A)** Experimental
943 design. **(B)** Representative FACS plots of p25 and DN1 T cells in the LN. Percentage of proliferating
944 **(C)** and CD44-expressing **(D)** p25 and DN1 T cells in the LN, lung, and spleen. N = 3 or 6 per
945 condition. Outliers were identified through Grubbs method with alpha=0.05 with one sample removed.

946 Data represented as mean ± SEM. Statistical analysis: 2-way ANOVA. *$p < 0.05$, **$p < 0.01$, ***$p <$
947 0.001, ****$p < 0.0001$.
948
949 **Fig. 4. Ag85B and MA dual loaded BCNs activate antigen-specific T cells without Ag85B**
950 **persistence. (A)** DLS analysis of blank BCN and Ag85B-MA-BCN. (**B-D**) hCD1Tg mice were IT
951 vaccinated with Ag85B-MA-BCN or BCN and CellTrace-labeled p25 and DN1 T cells were
952 adoptively transferred the next day. After 1 week, T cell activation and proliferation was measured. **(B)**
953 Representative FACS plots of p25 and DN1 T cells in the LN. Percentage of proliferating (**C**) and
954 CD44-expressing (**D**) p25 and DN1 T cells in the LN, lung, and spleen (N = 4 or 5). (**E-G**) hCD1Tg
955 mice were IT vaccinated with blank BCN or Ag85B-MA-BCN. 6 weeks later, CellTrace-labeled p25
956 and DN1 T cells were adoptively transferred, and T cell activation was measured after 1 week. **(E)**
957 Representative FACS plots of p25 and DN1 T cells in the LN. **(F)** Percentage of proliferating p25 and
958 DN1 T cells**. (G)** Percentage of CD44-expressing p25 and DN1 T cells in the LN and lung. (N = 4).
959 Data represented as mean ± SEM. Statistical analysis: 2-way ANOVA. ns = not significant, *$p<0.05$,
960 **$p<0.01$, ***$p<0.001$, ****$p< 0.0001$.
961
962 **Fig. 5. Route of vaccination or vector type do not affect antigen persistence.** hCD1Tg BMDCs
963 were pulsed with MA-BCN or MA at concentrations of 5 μg/mL and 10 μg/mL, respectively. hCD1Tg
964 mice were IT vaccinated with MA or MA-BCN pulsed BMDCs at 6 weeks or 1 week prior to the
965 adoptive transfer of CellTrace-labeled DN1 T cells. T cell activation and proliferation was measured 1
966 week after adoptive transfer. **(A)** Experimental design. **(B, C)** Percentage of proliferating **(B)** and
967 CD44-expressing **(C)** DN1 T cells in the LN, lung, and spleen of vaccinated mice. N = 4 per condition.
968 N = 4 per condition. hCD1Tg mice were vaccinated SC (subcutaneously) or IV (intravenously) with
969 blank BCN, MA-BCN, or attenuated Mtb strain and 6 weeks later CellTrace-labeled DN1 T cells were
970 adoptively transferred. **(D)** Representative FACS plots of DN1 T cells in the LN of mice vaccinated
971 with indicated conditions. **(E)** Percentage of proliferating DN1 T cells and **(F)** Percentage of CD44-
972 expressing DN1 T cells in the LN and spleen of mice vaccinated with Blank-BCN (SC), MA-BCN (IV

973 and SC), and attenuated Mtb. N = 3-5 per condition. Data represented as mean ± SEM. Statistical
974 analysis: 2-way ANOVA. ns = not significant, *p<0.05, **p<0.01, ***p<0.001, ****p<0.0001.
975
976 **Fig. 6. Persistent MA remains in part due to encapsulation inside alveolar macrophages and**
977 **activates T cells through DCs.** B6 or hCD1Tg mice were IT vaccinated with BCN loaded with a
978 hydrophobic fluorescent dye (DiD) at 6 weeks, 6 days, 48 hours, 24 hours, or 4 hours prior to the
979 experiment. LN, lung, and spleen were analyzed using **(A)** In Vivo Imaging System (IVIS). Single cell
980 suspension was then obtained and presence of DiD BCN was quantified in **(B)** total lung, and **(C)**
981 $CD45^-$ cells, neutrophils ($Ly6G^+$), alveolar macrophages ($CD11c^+SiglecF^+$), DCs ($CD11c^+$), monocytes
982 ($CD11b^+CD11c^-$), B cells ($CD19^+$), T cells ($CD3^+$), NK cells ($NK1.1^+$), eosinophils ($CD11c^-SiglecF^+$)
983 by flow cytometry. Gating strategy exemplified in **Suppl Fig 4**. hCD1Tg mice were IT vaccinated with
984 either BCN or MA-BCN. After 6 weeks, alveolar macrophages were enriched from lungs using anti-
985 SiglecF. Enriched or flow through cells were co-cultured with DN1 T cells in the presence or absence
986 of hCD1Tg-expressing BMDCs for 48 hours, and DN1 T cells activation was measured. **(D)**
987 Experimental design. **(E)** Percentage of CD25-expressing DN1 T cells. Data represented as mean ±
988 SEM. Statistical analysis: 2-way ANOVA. ns = not significant, *p<0.05, **p<0.01, ***p<0.001.
989
990 **Fig. 7**. **MA-BCN vaccination leads to DN1 T cell differentiation into T follicular helper-like T**
991 **cells**. Mixed bone marrow chimeric mice were created by adoptive transfer of DN1 bone marrow and
992 congenic CD45.1 hCD1Tg bone marrow to irradiated hCD1Tg mice. After 5 weeks, mice were
993 vaccinated with either MA-BCN or PBS, and DN1 surface marker expression was monitored in the
994 blood and in organs at 6 wks. **(A)** Experimental design. **(B)** Percent $CD44^+$ DN1 T cells in the blood at
995 various time points post vaccination. **(C)** Percent $CD44^+CD62L^+$ DN1 T cells in indicated organs at 6
996 weeks post vaccination. Memory ($CD44^+CD62L^+$) and naïve ($CD44^-CD62L^+$) DN1 T cells were sorted
997 from MA-BCN vaccinated hCD1Tg-DN1 BM chimeras at 6 weeks post vaccination and subjected to
998 RNAseq analysis. N=3 per condition **(D, E)** PCA of log fold change of gene expression for each T cell
999 subset was performed relative to internal naïve T cell control. **(F)** Relative expression of key T_{FH} cell
1000 and DEGs in memory subset. **(G)** Gene enrichment analysis of upregulated DEGs was performed

1001 using Metascape. **(H)** Representative FACS plots of DN1 T cells in the LN of mice. Percentage of **(I)**
1002 $CXCR5^{+}PD1^{+}$ or **(J)** $KI67^{+}$ DN1 T cells DN1 T cells in LN, lung, and spleen. N = 3-5 per condition.
1003 Data represented as mean ± SEM. Statistical analysis: 2-way ANOVA. *p<0.05, **p<0.01, ****p <
1004 0.0001.
1005
1006 **Fig. 8**. **Summary schematic illustrates MA antigen persistence and memory differentiation of**
1007 **antigen-specific T cells induced by vaccination with MA-loaded nanoparticle vaccine.**
1008 *Mycobacterium tuberculosis* (Mtb) derived mycolic acid (MA) lipid and Ag85B protein are
1009 encapsulated into bicontinuous nanosphere (BCNs) composed of PEG-*b*-PPS polymer. These MA-
1010 BCN or Ag85B-MA-BCN are used for intratracheal (IT) vaccination of human CD1 transgenic
1011 (hCD1Tg) mice. Following vaccination, dendritic cells (DCs) present the antigens, leading to the
1012 activation of CD1b-restricted MA-specific or MHCII-restricted Ag85B-specific T cells (DN1 or p25-
1013 specific T cells, respectively). Notably, MA can persist within alveolar macrophages and continue to
1014 activate MA-specific T cells even at 6 weeks post-vaccination. These MA-specific T cells have the
1015 capacity to differentiate into memory T cells with T follicular-like phenotype.

Figure 1

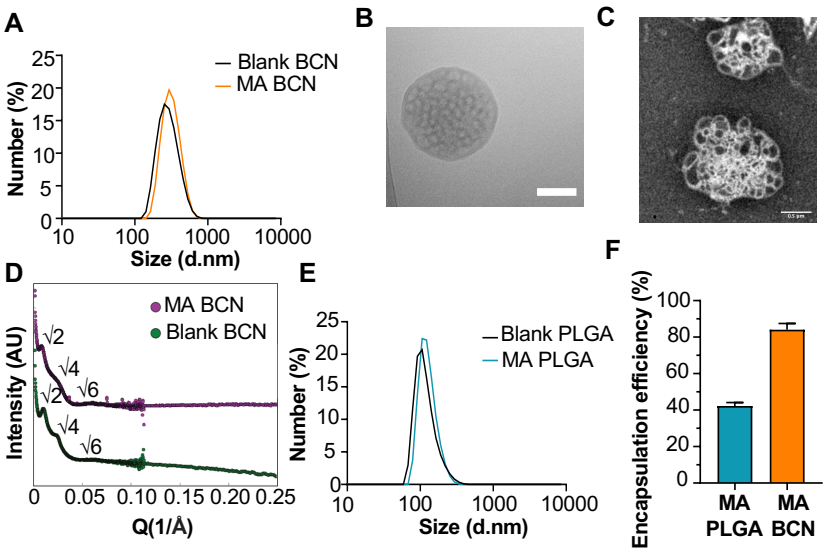
A
Blank BCN
MA BCN
Number (%)
Size (d.nm)
B
C
D
MA BCN
Blank BCN
Intensity (AU)
Q(1/Å)
√2
√4
√6
E
Blank PLGA
MA PLGA
Number (%)
Size (d.nm)
F
Encapsulation efficiency (%)
MA PLGA
MA BCN

Figure 2

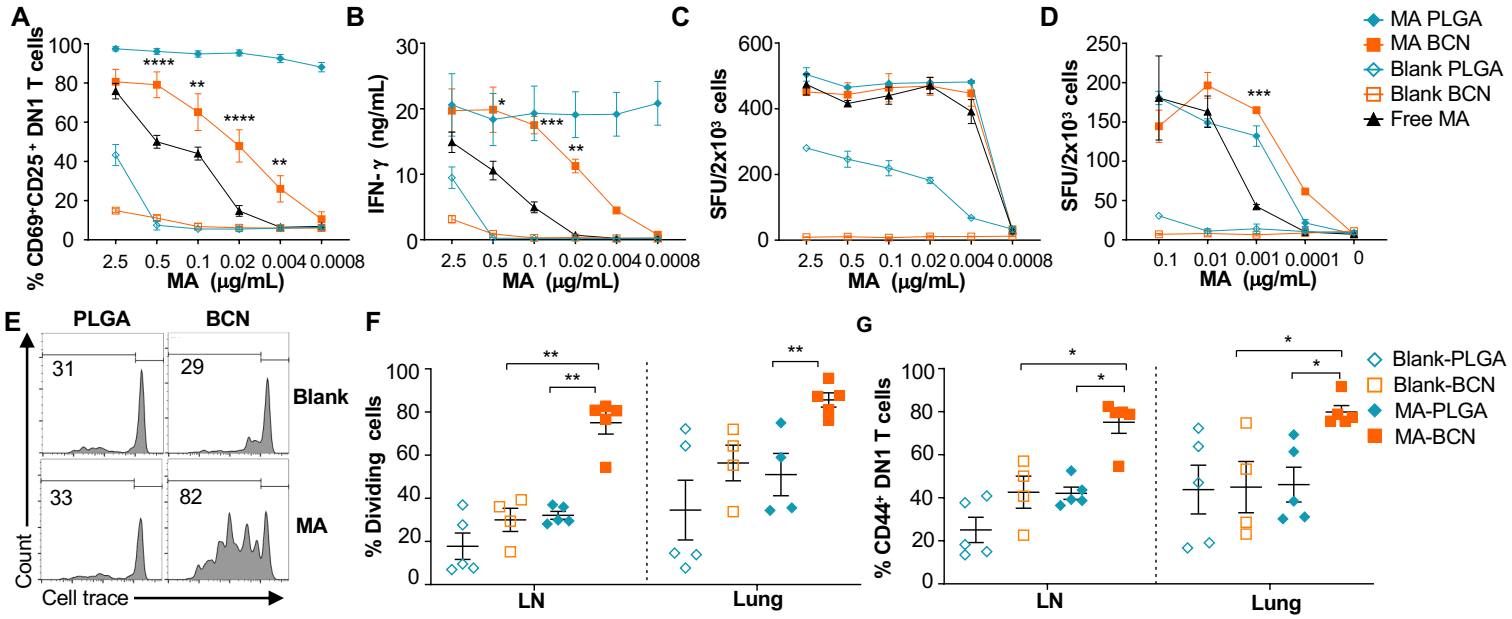
A
% CD69+CD25+ DN1 T cells
MA (µg/mL)
B
IFN-γ (ng/mL)
MA (µg/mL)
C
SFU/2x10³ cells
MA (µg/mL)
D
SFU/2x10³ cells
MA (µg/mL)
MA PLGA
MA BCN
Blank PLGA
Blank BCN
Free MA
E
PLGA
BCN
Blank
MA
Count
Cell trace
F
% Dividing cells
LN
Lung
G
% CD44+ DN1 T cells
LN
Lung
Blank-PLGA
Blank-BCN
MA-PLGA
MA-BCN

Figure 3

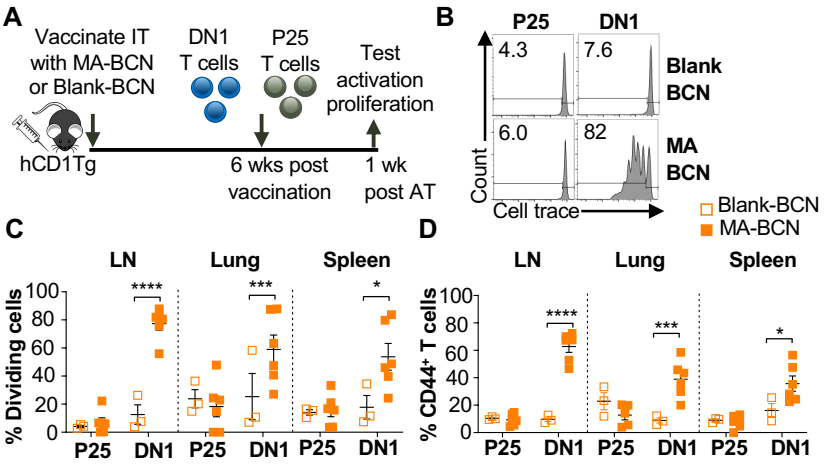
A
Vaccinate IT with MA-BCN or Blank-BCN
DN1 T cells
P25 T cells
Test activation proliferation
hCD1Tg
6 wks post vaccination
1 wk post AT
B
P25
DN1
4.3
7.6
6.0
82
Blank BCN
MA BCN
Count
Cell trace
Blank-BCN
MA-BCN
C
LN
Lung
Spleen
% Dividing cells
100
80
60
40
20
0
****
***
*
P25
DN1
D
% CD44+ T cells

Figure 4

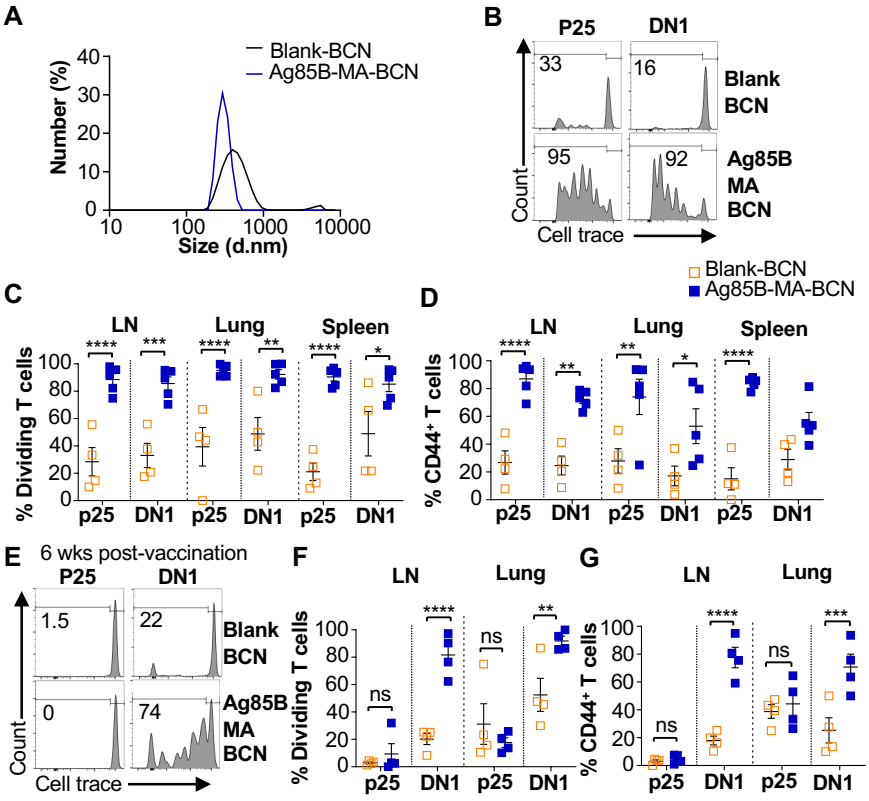
A
Blank-BCN
Ag85B-MA-BCN
Number (%)
Size (d.nm)
B
P25
DN1
33
16
95
92
Blank BCN
Ag85B MA BCN
Count
Cell trace
Blank-BCN
Ag85B-MA-BCN
C
LN
Lung
Spleen
% Dividing T cells
p25
DN1
D
% CD44+ T cells
E
6 wks post-vaccination
1.5
22
0
74
F
ns
G

Figure 5

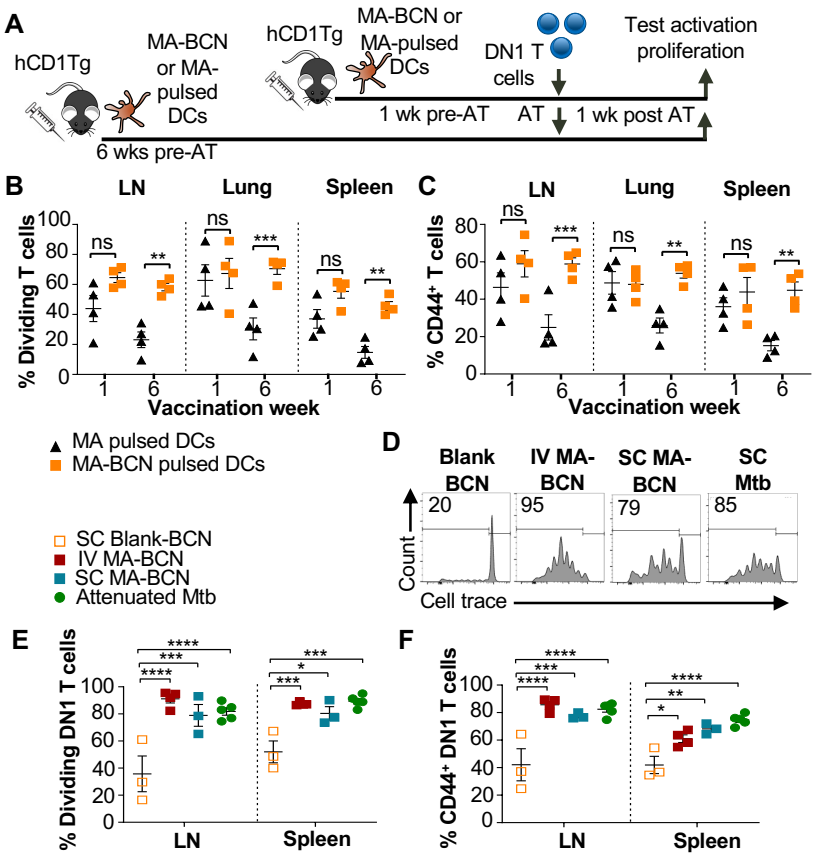
A
hCD1Tg
MA-BCN or MA-pulsed DCs
6 wks pre-AT
hCD1Tg
MA-BCN or MA-pulsed DCs
1 wk pre-AT
DN1 T cells
AT
1 wk post AT
Test activation proliferation
B
LN
Lung
Spleen
% Dividing T cells
Vaccination week
C
% CD44+ T cells
Vaccination week
MA pulsed DCs
MA-BCN pulsed DCs
D
Blank BCN
IV MA-BCN
SC MA-BCN
SC Mtb
20
95
79
85
Count
Cell trace
SC Blank-BCN
IV MA-BCN
SC MA-BCN
Attenuated Mtb
E
% Dividing DN1 T cells
LN
Spleen
F
% CD44+ DN1 T cells
LN
Spleen

Figure 6

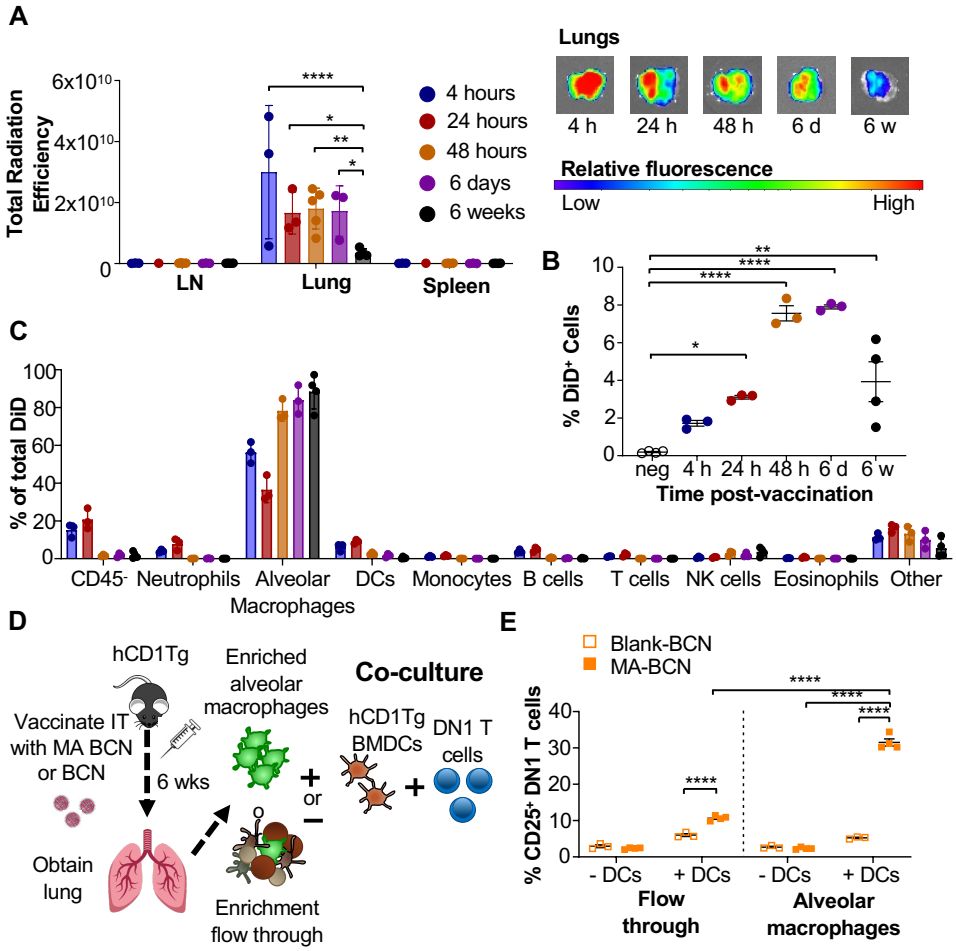
A
Total Radiation Efficiency
6x10¹⁰
4x10¹⁰
2x10¹⁰
0
****
*
**
*
LN
Lung
Spleen
4 hours
24 hours
48 hours
6 days
6 weeks
Lungs
4 h
24 h
48 h
6 d
6 w
Relative fluorescence
Low
High
B
% DiD⁺ Cells
10
8
6
4
2
0
**
****
****
*
neg
4 h
24 h
48 h
6 d
6 w
Time post-vaccination
C
% of total DiD
100
80
60
40
20
0
CD45⁻
Neutrophils
Alveolar Macrophages
DCs
Monocytes
B cells
T cells
NK cells
Eosinophils
Other
D
hCD1Tg
Vaccinate IT with MA BCN or BCN
6 wks
Obtain lung
Enriched alveolar macrophages
Enrichment flow through
+ or −
Co-culture
hCD1Tg BMDCs
+
DN1 T cells
E
Blank-BCN
MA-BCN
% CD25⁺ DN1 T cells
40
30
20
10
0
****
****
****
****
- DCs
+ DCs
- DCs
+ DCs
Flow through
Alveolar macrophages

Figure 7

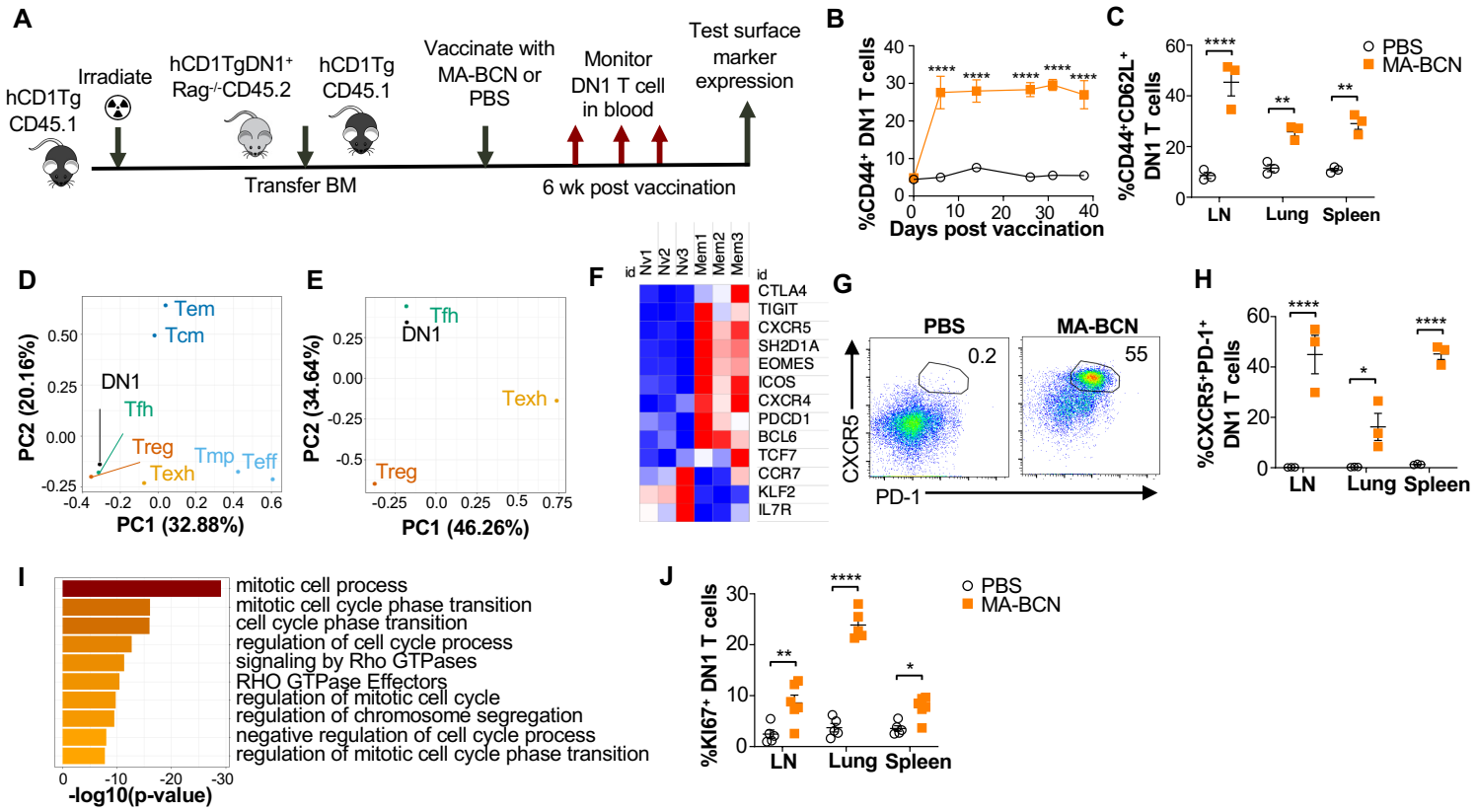
A
hCD1Tg CD45.1
Irradiate
hCD1TgDN1+ Rag-/-CD45.2
hCD1Tg CD45.1
Vaccinate with MA-BCN or PBS
Monitor DN1 T cell in blood
Test surface marker expression
Transfer BM
6 wk post vaccination
B
%CD44+ DN1 T cells
Days post vaccination
C
%CD44+CD62L+ DN1 T cells
PBS
MA-BCN
LN
Lung
Spleen
D
PC2 (20.16%)
PC1 (32.88%)
Tem
Tcm
DN1
Tfh
Treg
Tmp
Teff
Texh
E
PC2 (34.64%)
PC1 (46.26%)
Tfh
DN1
Texh
Treg
F
id
Nv1
Nv2
Nv3
Mem1
Mem2
Mem3
CTLA4
TIGIT
CXCR5
SH2D1A
EOMES
ICOS
CXCR4
PDCD1
BCL6
TCF7
CCR7
KLF2
IL7R
G
PBS
MA-BCN
0.2
55
CXCR5
PD-1
H
%CXCR5+PD-1+ DN1 T cells
LN
Lung
Spleen
I
mitotic cell process
mitotic cell cycle phase transition
cell cycle phase transition
regulation of cell cycle process
signaling by Rho GTPases
RHO GTPase Effectors
regulation of mitotic cell cycle
regulation of chromosome segregation
negative regulation of cell cycle process
regulation of mitotic cell cycle phase transition
-log10(p-value)
J
%KI67+ DN1 T cells
PBS
MA-BCN
LN
Lung
Spleen

Figure 8

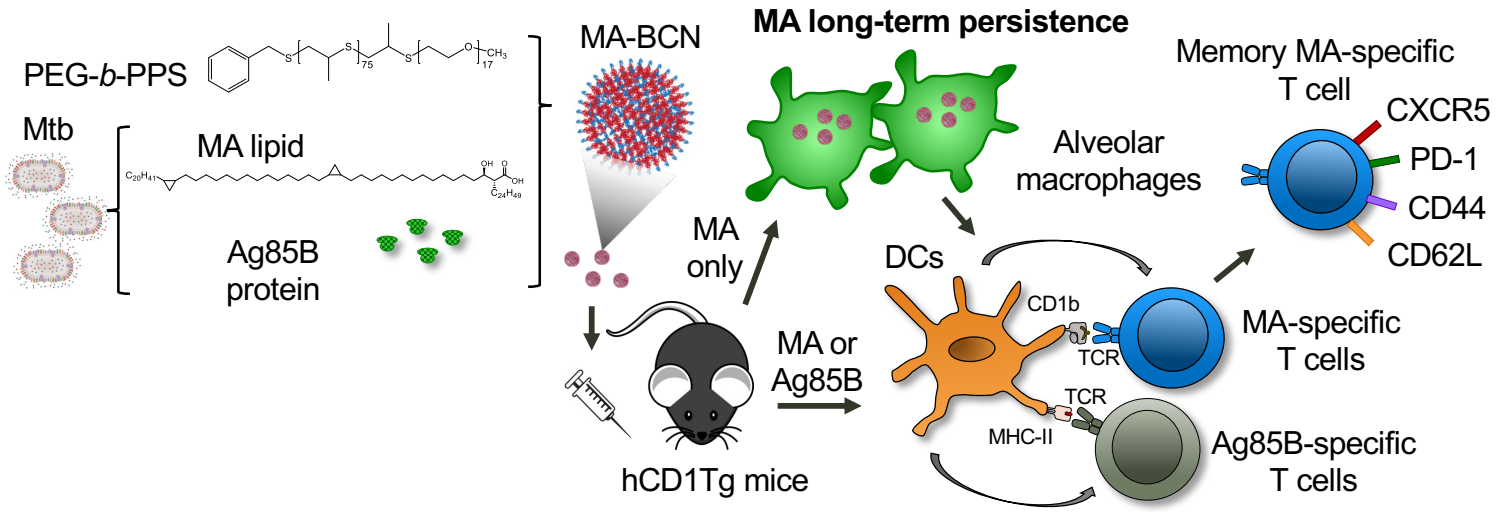
PEG-*b*-PPS
Mtb
MA lipid
Ag85B
protein
MA-BCN
MA long-term persistence
MA
only
Alveolar
macrophages
DCs
CD1b
TCR
TCR
MHC-II
MA or
Ag85B
hCD1Tg mice
Memory MA-specific
T cell
CXCR5
PD-1
CD44
CD62L
MA-specific
T cells
Ag85B-specific
T cells

Supplementary Figure Legends

Fig. S1. Physicochemical characterization of PLGA-NP. (A) CryoTEM image and DLS. **(B)** SAXS scattering curve fitted with a sphere model.

Fig. S2. Intracellular localization of PLGA-NP and BCN. (A) Representative confocal image of intracellular localization of PLGA or BCN (Texas red Dextran dye), lysosome (lysotracker), nucleus (NucBlue). **(B)** Quantification of co-localization of lysotracker with Texas red dye by Pearson correlation. (8 cells were analyzed per experiment, 3 independent experiments), ****$p<0.0001$.

Fig. S3. MA encapsulated by either BCN or MC formulation leads to lipid antigen persistence. hCD1Tg mice were IT vaccinated with MA-BCN or MA-MC at 6 weeks or 1 week prior to adoptive transfer of cell trace stained DN1 T cells. T cell activation and proliferation was measured 1 week after adoptive transfer. **(A)** Experimental diagram. **(B)** Percentage of proliferating DN1 T cells in LN, lung, and spleen. **(C)** Percentage of CD44-expressing DN1 T cells in the LN, lung, and spleen. N = 3 or 4 per condition. Data represented as mean ± SEM. ns = not significant, *$p<0.05$.

Fig. S4. P25-specific T cell activation and proliferation and bacterial burden in attenuated Mtb vaccination. hCD1Tg were SC vaccinated with attenuated Mtb. **(A)** Bacterial burden in the spleen and lung were determined at 2- or 6-weeks post vaccination. hCD1Tg mice were vaccinated with attenuated Mtb and after 6 weeks, CellTrace-labeled p25 T cells were adoptively transferred into the mice. After 1 week, T cell activation and proliferation was measured. (**B)** Representative FACS plots of in LN. **(C)** Percentage of proliferating P25 T cells in the LN and spleen. **(D)** Percentage of CD44-expressing P25 T cells in the LN and spleen (N = 5).

Fig. S5. Gating strategy for analyzing biodistribution of BCN in the lung. Lung single cell suspension was gated as follows: $CD45^-$ cells, neutrophils ($Ly6G^+$), alveolar macrophages

28 (CD11c^{+}SiglecF^{+}), DCs (CD11c^{+}), monocytes (CD11b^{+}CD11c^{-}), B cells (CD19^{+}), T cells (CD3^{+}), NK
29 cells (NK1.1^{+}), and eosinophils (CD11c^{-}SiglecF^{+}).
30
31 **Fig. S6. Representative FACS plot of alveolar macrophages within enriched and flow through**
32 **fractions.**
33
34 **Fig. S7. Memory and naïve DN1 T cells display distinct gene expression profiles.** Memory
35 (CD44^{+}CD62L^{+}) and naïve (CD44^{-}CD62L^{+}) DN1 T cells were sorted from LNs of MA-BCN
36 vaccinated hCD1Tg-DN1 BM chimeras at 6 weeks post vaccination and subjected to RNAseq analysis
37 **(A)** Representative figure of CD44 and CD62L expression in DN1 T cells in LN, lung, and spleen. **(B)**
38 MA plot representing memory vs naïve analysis. **(C)** PCA of normalized counts. N=3 per condition.
39
40

Supplementary Figure 1

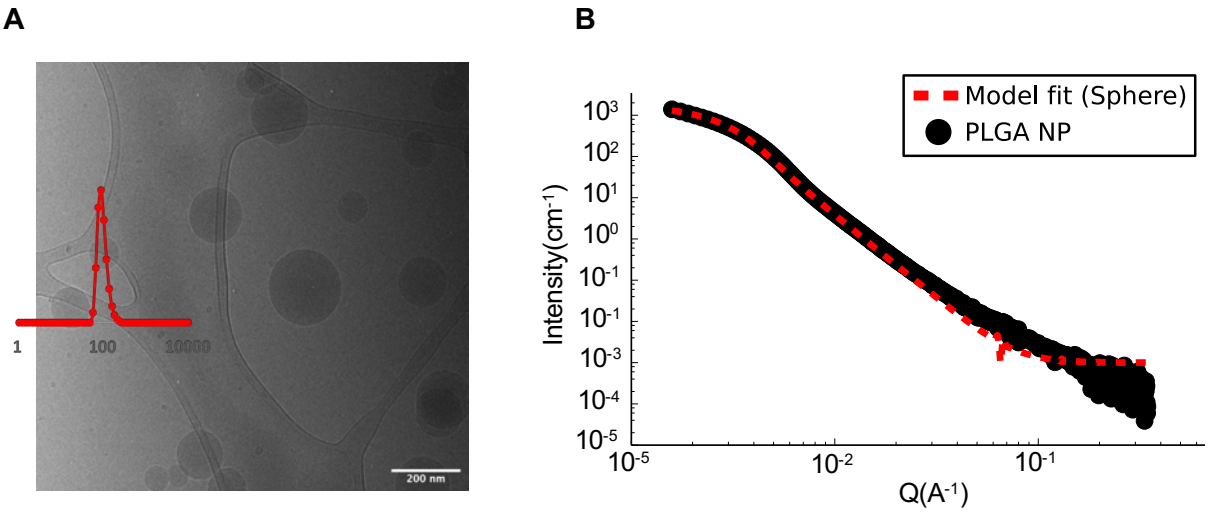

Supplementary Figure 2

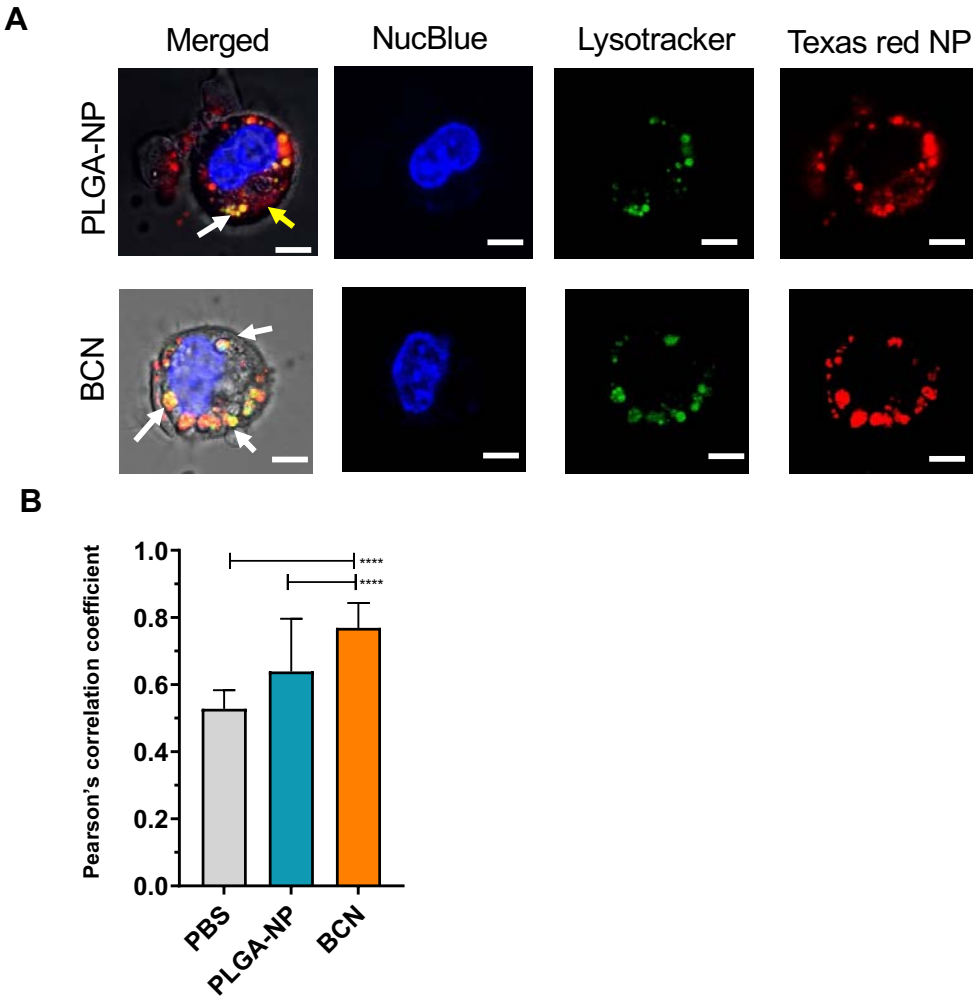

Supplementary Figure 3

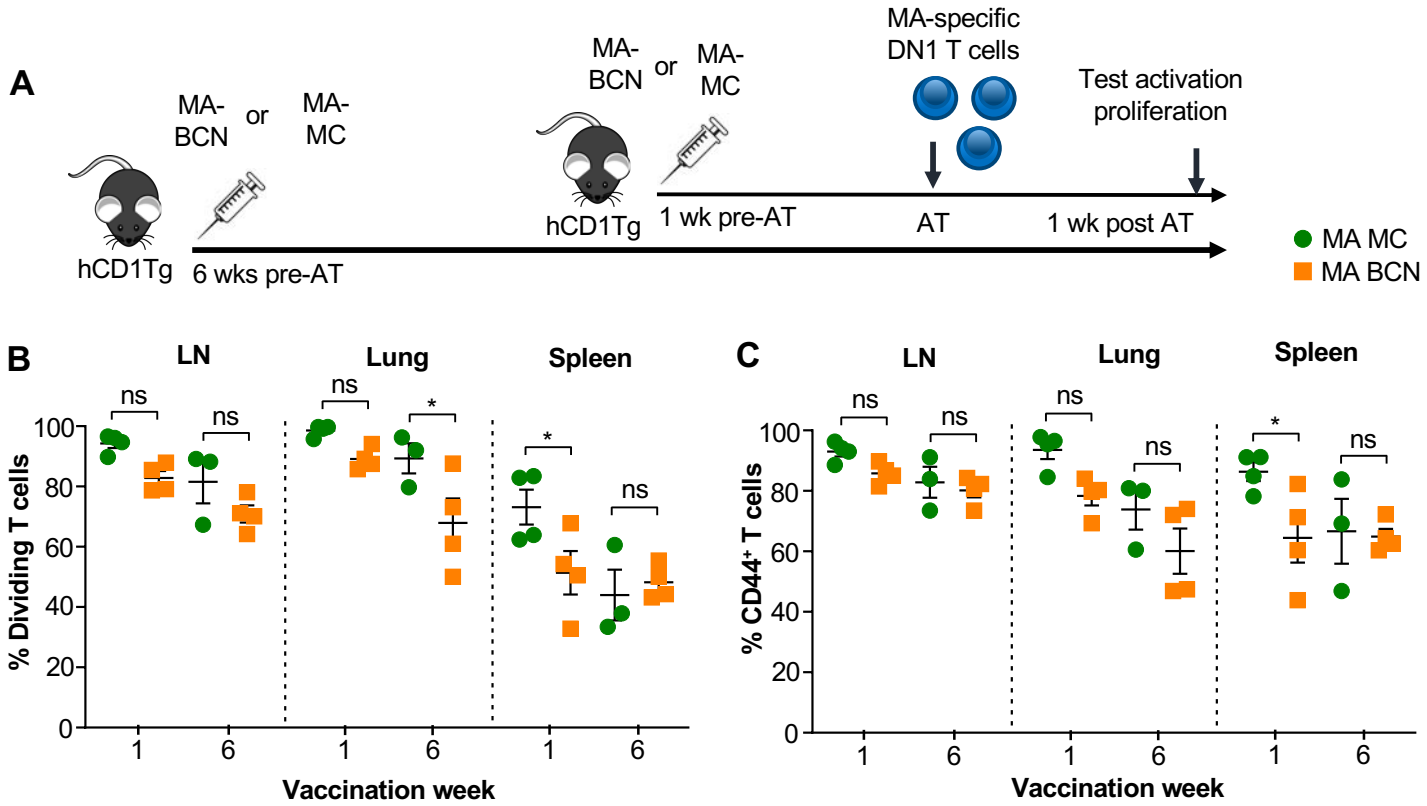

Supplementary Figure 4

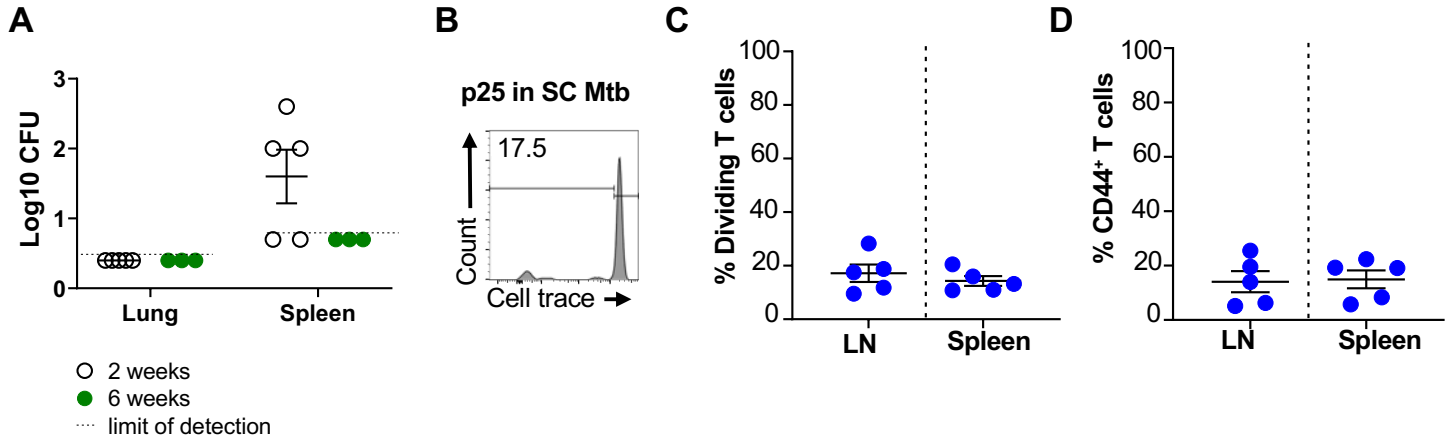

Supplementary Figure 5

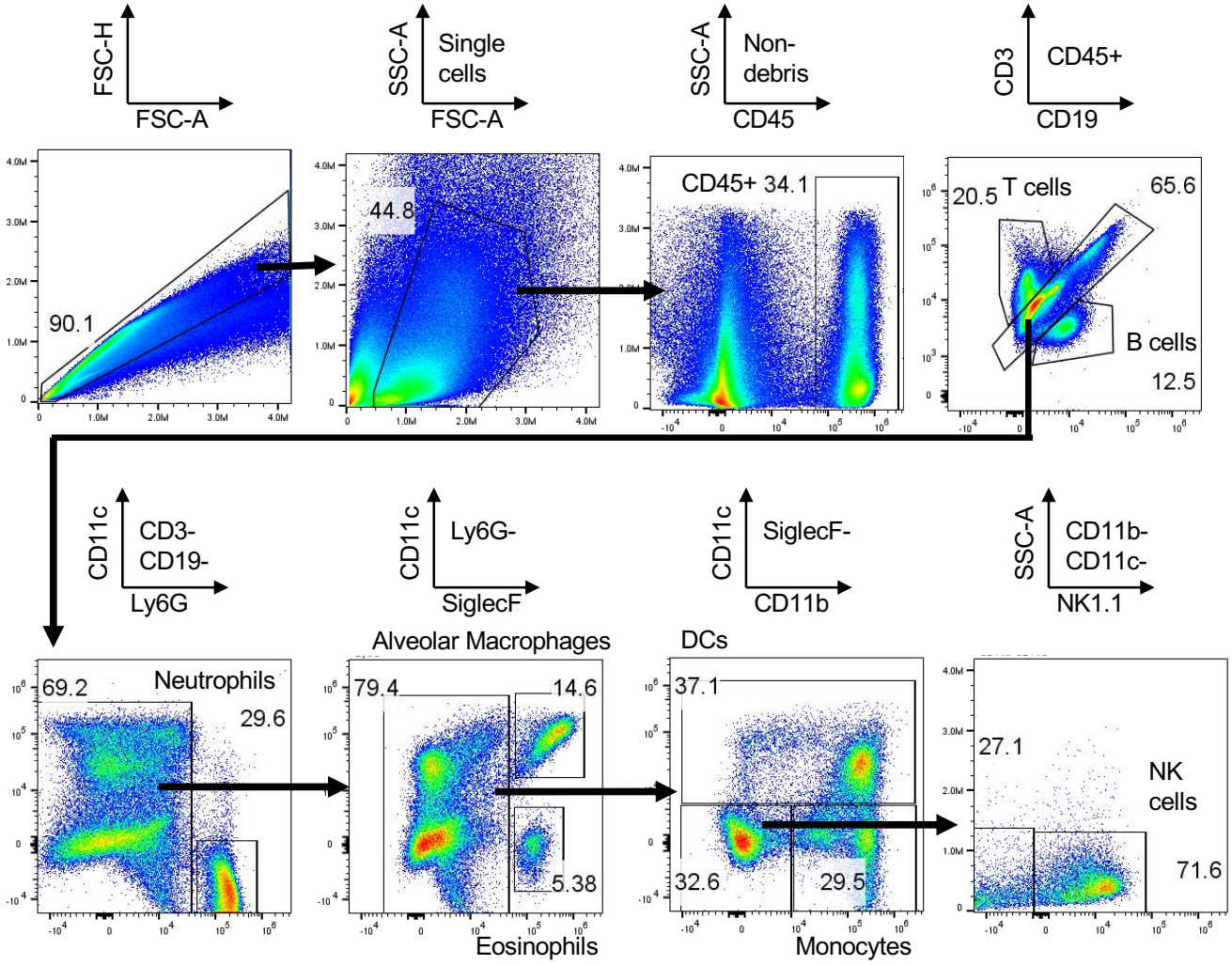

Supplementary Figure 6

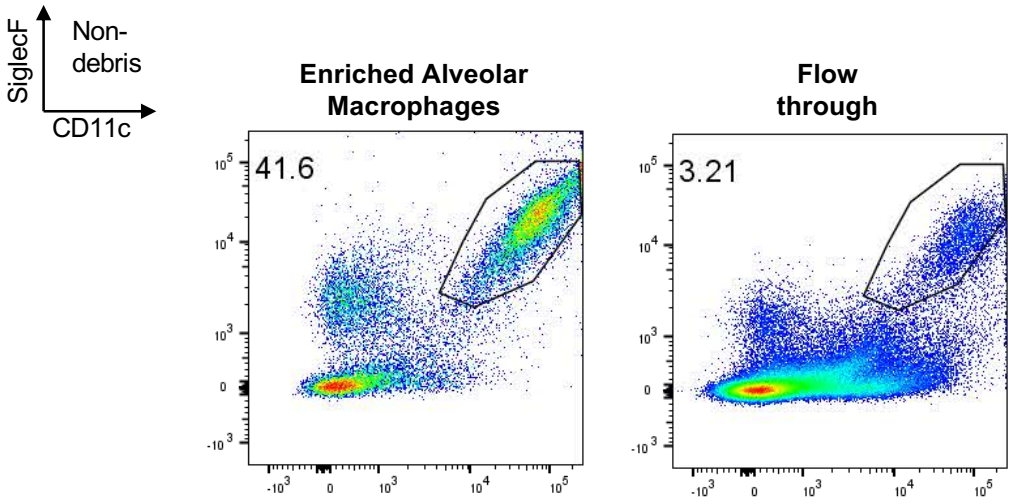
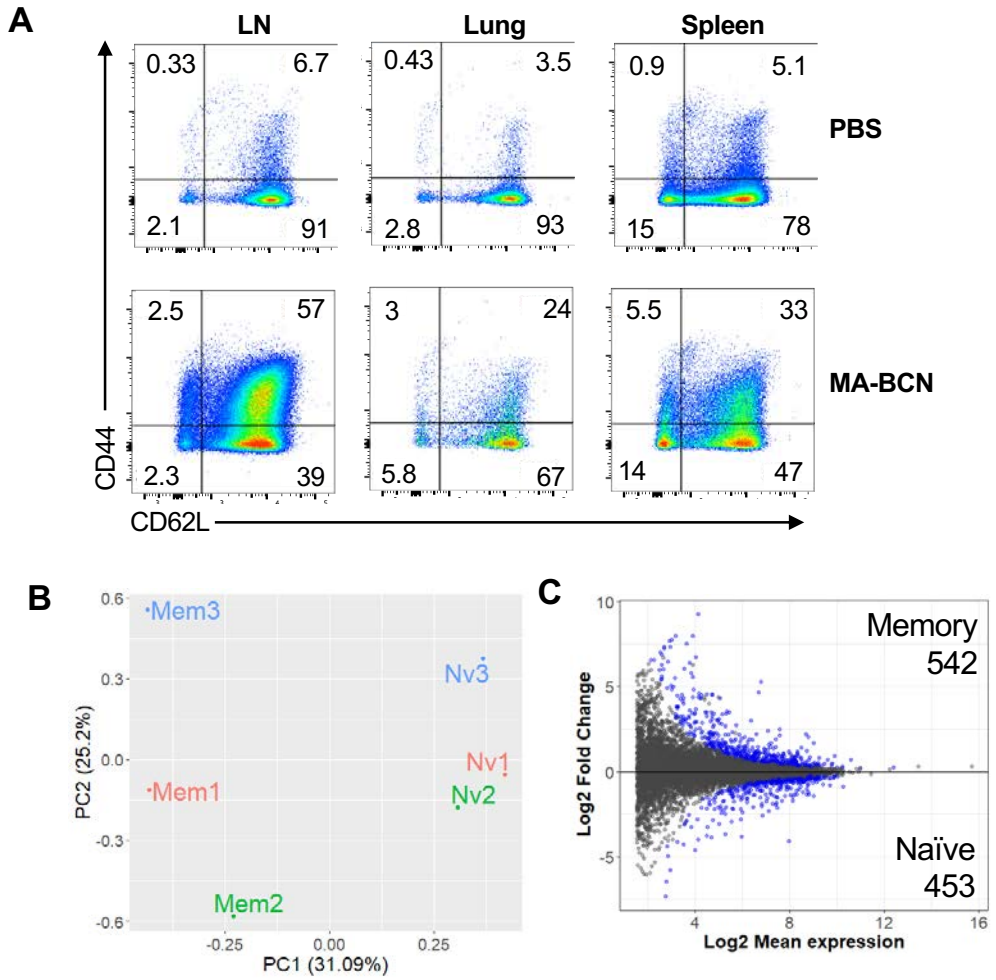
Supplementary Figure 7